Senescence in yeast is associated with chromosome XII cleavage rather than ribosomal DNA circle accumulation

Andre Zylstra[1,2], Dorottya Horkai[1,3], Hanane Hadj-Moussa[1,4], Baptiste Piguet[1,5] and Jonathan Houseley[1,*]

[1] Epigenetics Programme, Babraham Institute, Cambridge, CB22 3AT

[2] ORCID: 0000-0001-9762-6728. Present address: Molecular Systems Biology, Groningen Biomolecular Sciences and Biotechnology Institute, University of Groningen, 9747 AG, the Netherlands

[3] ORCID: 0000-0001-9430-1864. Present address: Abcam plc, Biomedical Campus, Discovery Drive, Cambridge, CB2 0AX

[4] ORCID: 0000-0002-3338-9046

[5] ORCID: 0000-0001-7077-2266. Present address: Research and Teaching Biology Department, ENS Paris-Saclay, Ile-De-France, 91190

*Corresponding author: jon.houseley@babraham.ac.uk, ORCID: 0000-0001-8509-1500

Abstract

The massive accumulation of extrachromosomal ribosomal DNA circles (ERCs) in yeast mother cells has been long cited as the primary driver of replicative ageing. ERCs arise through ribosomal DNA (rDNA) recombination and a wealth of genetic data connects rDNA instability to shortened lifespan and other ageing pathologies. However, we understand little about the molecular effects of ERC accumulation. Here we analysed the widespread disruption of gene expression that accompanies yeast ageing, and unexpectedly found this to be independent of ERCs. Furthermore, we found no evidence of gene expression differences in the presence of ERCs that might indicate stress responses or metabolic feedback. Accumulation of Tom70-GFP, a marker for the onset of cell division defects at the Senescence Entry Point (SEP), also correlated poorly to ERC abundance but displayed a transcriptomic signature separable from age. This signature is dominated by copy number amplification of a region of chromosome XII between the rDNA and the telomere (ChrXIIr) which arises in aged cells due to rDNA instability, but through a different mechanism to ERCs. Our findings implicate ChrXIIr, rather than ERCs, as the primary driver of senescence during budding yeast ageing.

Key words

Yeast; ageing; senescence; ribosomal DNA; rDNA; extrachromosomal rDNA circle; ERC; chromosome fragmentation

Introduction

Replicative ageing in the budding yeast *Saccharomyces cerevisiae* is a widely used model of ageing in dividing cells (He et al., 2018; Janssens and Veenhoff, 2016a; Kaeberlein, 2010). Under this paradigm, age is the number of budding events undergone by a mother cell and lifespan is the total number of divisions prior to a permanent loss of replicative potential (Mortimer and Johnston, 1959). Long-term imaging shows that cell cycle duration remains constant for most of the replicative lifetime but lengthens dramatically in the last few divisions (Fehrmann et al., 2013; Janssens and Veenhoff, 2016b; Sarnoski et al., 2018). This indicates a period of pathological ageing precedes loss of replicative viability, although the cause of this transition to a pathological ageing state is still debated.

Ageing cells display a spectrum of molecular phenotypes including dramatic changes in gene expression. This has been attributed to a loss of transcriptional repression due to histone depletion (Feser et al., 2010; Hu et al., 2014), the induction of a widespread but defined environmental stress response (Gasch et al., 2000; Hendrickson et al., 2018; Lesur and Campbell, 2004; Yiu et al., 2008) and the uncoupling of translation from mRNA abundance (Janssens et al., 2015). Whatever the cause, ageing yeast undergo widespread induction of coding and non-coding loci that are normally repressed for RNA polymerase II transcription during vegetative growth, and increase expression of stress and environmental response factors while the abundance of mRNAs encoding translation and ribosome biogenesis components is decreased (Cruz et al., 2018; Hendrickson et al., 2018; Hu et al., 2014; Pal et al., 2018; Yiu et al., 2008). Similarly, and perhaps consequently, the proteome becomes dysregulated, aggregation prone, and increasingly uncoupled from the transcriptome, gene expression becomes unresponsive and the metabolome shifts towards reduced growth and substrate uptake (Janssens et al., 2015; Leupold et al., 2019; Moreno et al., 2019; Neurohr et al., 2018). Interestingly, single-cell techniques have revealed that the onset of senescence is a discrete process initiated abruptly at the senescence entry point (SEP) (Fehrmann et al., 2013; Morlot et al., 2019). After the SEP, cells exhibit an extended G1 phase marked by intense foci of the tagged mitochondrial membrane protein Tom70-GFP and low levels of cyclin Cln1. However, cell growth does not pause, leading to rapid cell size expansion and pathological cytoplasmic dilution coincident with nuclear and nucleolar growth (Fehrmann et al., 2013; Moreno et al., 2019; Morlot et al., 2019; Neurohr et al., 2019; Sarnoski et al., 2018).

The most prominent theory of yeast ageing focuses on accumulation of ERCs, which arise during homologous recombination within the highly repetitive rDNA locus (Defossez et al., 1999; Park et al., 1999; Sinclair and Guarente, 1997). ERCs are replicated in each cell cycle and are asymmetrically retained in mother cells at mitosis by the SAGA and TREX-2 complexes, such that ERC copy number rises exponentially during ageing to the point that effective genome size increases 30-40% in 24 hours (Cruz et al., 2018; Denoth-Lippuner et al., 2014; Morlot et al., 2019; Shcheprova et al., 2008; Sinclair and Guarente, 1997). Due to this behaviour, ERCs are very plausible 'ageing factors' that arise early in ageing and later cause nucleolar fragmentation (Mansisidor et al., 2018; Sinclair and Guarente, 1997; Sinclair et al., 1997). Important components of this theory are Sir2, the eponymous member of the highly conserved sirtuin protein deacetylase family, and Fob1, which localises to the rDNA replication fork barrier (RFB) site. Fob1 stalls replication forks at the RFB and averts head-on collision with RNA polymerase I, but resolution of the stalled forks can be recombinogenic through repair events leading to ERC formation (Defossez et al., 1999; Kobayashi et al., 1998; Kobayashi and Horiuchi, 1996). In support of the ERC theory, *SIR2* deletion destabilises the rDNA, promotes ERC accumulation and rDNA copy number variation, and shortens yeast lifespan, whereas *FOB1* deletion or *SIR2* overexpression extend lifespan (Defossez et al., 1999; Kaeberlein et al., 1999). ERC-encoded non-coding RNAs are abundantly expressed by RNA polymerase II with a concomitant accumulation of activating epigenetic marks such as H3K4me3, while the additional ribosomal DNA genes are transcribed by RNA polymerase I (Cruz et al., 2018; Morlot et al., 2019; Pal et al., 2018). As such, it is not hard to imagine that titration of nuclear and nucleolar factors by thousands of ERCs could imbalance the protein coding transcriptome and/or ribosome synthesis.

Anti-ageing interventions with cross species efficacy, such as caloric restriction and mTOR inhibition, also reduce rDNA instability and recombination through Sir2 (Ha and Huh, 2011; Jack et al., 2015; Lin et al., 2000; Salvi et al., 2013). Remarkably, there are indications that rDNA instability and copy number variation might be relevant to animal ageing and pathology as rDNA copy number variation has been reported during *Drosophila* and mouse ageing (Lu et al., 2018; Watada et al., 2020), in human neurodegenerative disorders (Hallgren et al., 2014), and in cancer (Stults et al., 2008; Valori et al., 2020; Wang and Lemos, 2017; Xu et al., 2017). Circular DNAs containing rDNA sequence have also been observed in *Drosophila* and human cells (Cohen et al., 2010; Cohen et al., 2003). However, although accumulation of ERCs in ageing yeast was first reported a quarter of a century ago there remains a conspicuous lack of analogous data for any other model organism (Sinclair and Guarente, 1997). Nonetheless, recent publications showing a tight connection between ERC accumulation and ageing phenotypes in yeast strongly suggest that ERCs are the proximal cause of age-related cell cycle disruption and senescence. Neurohr *et al*. observed that mother cells are rejuvenated through rare events in which the entire ERC complement is transmitted to a daughter cell, Ünal *et al*. observed that ERCs are compartmentalised and degraded during meiosis in aged cells (King et al., 2019; Ünal et al., 2011), while Morlot *et al*. reported that cell cycle disruption and the SEP coincide with exponential ERC accumulation and concomitant excess rDNA transcription (Morlot et al., 2019; Neurohr et al., 2018). Furthermore, Meinema *et al.* recently reported that extended association of ERCs with nuclear pore complexes can promote the progressive decay of nuclear pore complexes that occurs during ageing in yeast (Meinema et al., 2022; Rempel et al., 2019).

These studies strongly suggest that ERC accumulation is pathological, but there is little mechanistic evidence of how ERC-dependent pathology may be mediated. We hypothesised that ERC accumulation causes age-linked dysregulation of gene expression and thereby promotes the transition to senescence at the SEP. To test this, we used mutants in ERC formation and retention to define the effect of ERCs on mRNA abundance and senescence, but unexpectedly found that neither process was associated with ERCs. Instead we implicate a large fragment of chromosome XII (ChrXIIr) as the unanticipated driver of ageing phenotypes in yeast.

Results

To investigate the role of ERC accumulation during replicative ageing in *S. cerevisiae*, we examined aged mutant cells that fail to accumulate ERCs during ageing. Homologous recombination-deficient *rad52*Δ cells cannot form ERCs, whereas *spt3*Δ and *sac3*Δ cells lack components of SAGA and TREX-2 so cannot retain ERCs in mother cells (Figure 1A) (Denoth-Lippuner et al., 2014; Park et al., 1999). By studying mutants in different pathways required for age-linked ERC accumulation, we aimed to separate effects caused by ERCs from unrelated effects of individual mutations.

For purification of aged cells we employed the Mother Enrichment Program (MEP) devised by Lindstrom and Gottschling (Lindstrom and Gottschling, 2009). MEP cells proliferate normally until β-estradiol is added to a culture, after which all new-born daughter cells are rendered inviable. This allows mother cells to reach advanced replicative age in batch culture without proliferation of young cells depleting media components. Mother cell walls are labelled with reactive biotin when young which allows recovery of the same cells on magnetic streptavidin beads at aged time points after fixation (Figure 1B).

Not all mutations that alter ERC abundance in young cells have equivalent effects in aged cells. For example, young *fob1*Δ mutant cells contain fewer ERCs, but ERC abundance in aged diploid *fob1*Δ MEP cells hardly differs from wild type (Figure S1A)(Lindstrom et al., 2011). We therefore confirmed ERC abundance in all three mutants by southern blot. Reassuringly, deletion of *RAD52* in the MEP background abrogated ERC accumulation (Defossez et al., 1999; Park et al., 1999), whilst deletion of *SPT3* or *SAC3* dramatically reduced ERC accumulation during ageing relative to wild type (Figure S1B)(Denoth-Lippuner et al., 2014).

Age-linked transcriptomic dysregulation is independent of ERCs

The RNA polymerase II transcriptome should provide a sensitive readout of the impact of ERCs on the ageing process, reporting both changes in overall distribution of mRNA abundance and also the expression of individual genes. Individual gene expression differences were predicted to be particularly informative, indicating stress response pathways and/or metabolic feedback circuits activated due to pathological impacts of ERC accumulation.

Poly(A)+ RNA-seq libraries were derived from MEP wild-type, *spt3*Δ and *sac3*Δ cells in triplicate and *rad52*Δ cells in duplicate. Cells were harvested at log phase and after 24 and 48 hours of ageing, times at which ~100% and ~30-40% of wild-type cells remain viable respectively (Figure 1B)(Cruz et al., 2018; Lindstrom and Gottschling, 2009). Expression of 1186 genes enriched for *carbohydrate metabolism*, *respiration* and *cell wall organisation* increased significantly at 48 hours compared to log phase in wild type, while 870 genes enriched for *ribosome synthesis* and *translation* decreased significantly, all of which is highly consistent with previous ageing gene expression studies and supports the reliability of our dataset (DESeq2, Benjamini-Hochberg (BH) corrected false discovery rate (FDR) < 0.05, $\log_2$-fold change threshold ± 0.5)(Figure S1C)(Cruz et al., 2018; Hendrickson et al., 2018; Hu et al., 2014).

We performed Principal Component Analysis (PCA) on the full RNA-seq dataset and found that samples segregated by age on PC1 (47% of variance) and by genotype on PC2 (12% of variation). PC1 score increased with age in all genotypes and the progression was strikingly similar between wild type and *spt3*Δ (Figure 1C, compare grey and purple). The 24 and 48-hour transcriptomes of *rad52*Δ cells clustered together, consistent with these very short-lived cells having reached the end of their replicative life span by 24 hours (Park et al., 1999); we did not observe cell death from 24 to 48 hours and the increased chronological age of the non-dividing cells evidently did not impact the transcriptome (Figure 1C, green). In contrast, the *sac3*Δ transcriptome progressed on PC1 both from log to 24 and from 24 to 48 hours, but less so than wild type - consistent with slower but continuous division (Figure 1C, orange).

Yeast cells are reported to undergo genome-wide transcriptional de-repression during ageing, particularly of low-expressed genes (Hu et al., 2014). This is clearly visible in MA plots, which display the change in expression with age of each gene as a function of the average expression of that gene (Figure 1D). In wild type, genes with low average expression are strongly induced with age, genes with intermediate expression change little relative to average, and abundant mRNAs decrease relative to average, imparting a characteristic skew away from horizontal to the distribution that can be quantified by the slope of a line of best fit (Figure 1D, dotted line). The MA plot for *spt3*Δ is essentially identical to wild type (Figure 1D, compare grey and purple), and a similar effect is observed in *rad52*Δ and *sac3*Δ (Figure 1D, compare grey to green and orange).

In contrast to our expectations, we therefore conclude that the dramatic remodelling of mRNA abundance which accompanies yeast replicative ageing is completely independent of the massive genomic and epigenomic changes resulting from ERC accumulation.

ERC accumulation exerts minimal effects on individual genes

Bulk transcriptome properties could mask differences in the behaviour of large numbers of genes. However, for the set of genes significantly differentially expressed between log phase and 48 hours in wild type (DESeq2, BH-corrected FDR < 0.05, $\log_2$-fold change threshold ± 0.5), the direction and magnitude of mRNA abundance change during ageing correlates strongly between wild type and mutants (Figure 2A). This is highly consistent with other studies showing common age-related transcriptional patterns between wild type and various mutant genotypes (Cruz et al., 2018;

Hendrickson et al., 2018). This analysis further shows that broad age-related transcriptional changes are robustly conserved regardless of ERC accumulation.

We next looked for changes in more specific processes or pathways which might be ERC-dependent. We performed pair-wise differential expression analyses between wild type and each mutant for 48 hour-aged samples and looked for genes consistently over- or under-expressed in all mutants lacking ERCs (DESeq2, BH-corrected FDR < 0.05, $\log_2$-fold change threshold ± 0.5). However, this very conservative approach only identified 10 genes and worryingly one of these was *TRP1*, the marker used for deleting *SPT3*, *SAC3* and *RAD52*. We therefore turned to a linear modelling approach with greater statistical power, and to control for *TRP1* auxotrophy added three replicate ageing time-courses for a MEP wild-type strain with the *TRP1* locus repaired.

Using this expanded dataset, we performed a differential expression analysis including all samples in a linear model design (Love et al., 2014). Samples were stratified on four categorical independent variables: Genotype (wild type, *spt3*Δ, *rad52*Δ, *sac3*Δ), *TRP1* auxotrophy (present, not present), Age (log phase, 24 hours, 48 hours), ERC accumulation level (low, high). 24 hour and 48 hour wild-type samples were classified as 'high' ERC level and all other samples were classified as 'low'. Of 161 genes differentially expressed between 'high' and 'low' ERC levels (DESeq2, BH-corrected FDR < 0.05, $\log_2$-fold change threshold ± 0.5), only 3 genes (*CSS1*, *PHO11* and *PHO12*) were significantly downregulated at high ERC levels, while 158 genes were significantly upregulated. 6 genes were differentially expressed depending on whether functional *TRP1* was present, but these did not overlap with genes differentially expressed due to ERC level.

Following hierarchical clustering, we split the 158 candidate ERC-induced genes into two large clusters, which most noticeably differ in *rad52*Δ datasets (Figure 2B). Cluster 1 genes were mostly highly expressed in *rad52*Δ and low in *spt3*Δ and *sac3*Δ (Figure 2B, top). This cluster includes annotations covering the regions of chromosomal rDNA and ERCs that are normally silenced by Sir2 (Bryk et al., 2002; Houseley et al., 2007; Li et al., 2006; Smith and Boeke, 1997). Age-related transcriptional induction of RNA polymerase II-transcribed non-coding RNAs within rDNA repeats was very low in all three low-ERC mutants but increased dramatically with age in wild type, coherent with high transcriptional activity of these regions on ERCs (Figures 2B, S2A)(Pal et al., 2018). In fact, the IGS1-F non-coding RNA was induced sufficiently to become the most abundant poly(A)+ RNA in aged wild-type cells (Figure S2B). Discovery of these transcripts validates the linear model approach, which essentially identifies genes as differentially expressed based on ERC level if they change less with age in the mutants than in the wild type. Remaining cluster 1 genes are dominated by retrotransposable elements (23 / 46 genes), expression of which is known to increase in *rad52*Δ and decrease in *spt3*Δ (Rattray et al., 2000; Winston et al., 1984). These follow the expected genotype-specific behaviour, which makes it unlikely that retrotransposable elements are *bona fide* ERC-induced transcripts.

In contrast, cluster 2 is largely composed of single copy protein coding genes, functionally enriched for *negative regulation of ATPase activity*, *negative regulation of hydrolase activity* and *cell wall organisation*. However, two lines of reasoning lead us to conclude these genes and ontologies are not relevant for ERC accumulation. Firstly, the DESeq2 linear model estimates the mean $\log_2$ contribution of each model factor (ERC level, age, genotype, *TRP1* auxotrophy) to the expression of each gene relative to a baseline of expression at log phase in wild type. It is notable that the median model coefficient for 'high' ERC level in cluster 2 genes is not outstanding compared to age and genotype (Figure S2C). This indicates that ERCs are, at most, a mid-ranking contributor to observed expression change even among the set of genes called as significantly upregulated based on 'high' ERC level. Secondly, as noted above, the linear modelling approach tends to assign gene expression changes to ERC level if a given gene changes consistently differently with age in mutants relative to wild type. However, the greatest difference in expression among cluster 2 genes between the mutants and the wild type is at log phase, prior to ERC accumulation, and this difference almost disappears in aged samples (Figure 2C). In other words, reduced induction of these genes with age (and hence expression being classified as ERC-dependent) results from all three mutants coincidentally causing

increased log-phase expression such that the increase with age is lessened, rather than ERCs causing the induction observed in aged wild-type cells.

Heterochromatic regions silenced by Sir2 followed the behaviour of ERC regulated transcripts (rDNA and mating type loci are in cluster 1), so we asked whether titration of Sir2 by ERCs can explain the reported age-linked induction of Sir2-regulated protein coding genes (Kaeberlein et al., 1999). We examined the DESeq2 linear model coefficients for the genes determined by Ellahi *et al*. to be repressed by the SIR complex, of which Sir2 is the active deacetylase (Ellahi et al., 2015). The 40 Sir2-regulated genes in our dataset mostly undergo age-related induction (Figure 2D), but the model coefficients for 'high' ERC level and 48-hour age, interpretable as the component of $\log_2$ fold change in expression attributable to ERC accumulation and to age, were 0.7 ± 1.3 and 1.8 ± 1.7 respectively (median ± interquartile range, Figure S2D). By comparison, these values for the cluster 2 genes were 1.7 ± 1.4 (for 'high' ERC level) and 1.5 ± 1.5 (for 48-hour age). Therefore, our data is consistent with ERC accumulation contributing to the de-repression of Sir2-regulated genes, but to a lesser extent than the de-repression of the same genes that occurs due to the ERC-independent age-linked dysregulation of gene expression.

Overall, despite the vast accumulation of ERCs during ageing and the resultant massive production of poly-adenylated non-coding RNA, we have been unable to identify protein coding genes for which we can conclude that the change in mRNA abundance during ageing is primarily driven by ERC accumulation.

ERC accumulation is not the only pathway to the SEP

ERC accumulation immediately precedes the SEP, which is marked by formation of very bright foci of the mitochondrial outer membrane protein Tom70-GFP in G1 (Fehrmann et al., 2013; Morlot et al., 2019). Yeast cells also undergo growth after entering the SEP to a point that cytoplasmic dilution could induce dysfunction (Neurohr et al., 2019), but it is unclear whether ERCs contribute to this growth. Both cell size and Tom70 foci formation can be quantified by imaging, so we set up a high-throughput assay using the Amnis ImageStream® flow cytometry system to image hundreds of individual MEP cells from purified aged MEP populations (see associated manuscript Horkai and Houseley).

Fluorescence images of Tom70-GFP were captured to assess onset of the SEP, with ribosome component Rpl13a-mCherry as a control that does not accumulate substantially or form foci during ageing in wild type (Janssens and Veenhoff, 2016b). Brightfield and wheat germ agglutinin (WGA) stained images were also acquired for each cell; cell area is calculated from brightfield while WGA intensity forms a quantitative marker of replicative age that correlates with manual bud scar counts in wild type and *spt3*Δ, with a slight underestimate in *rad52*Δ (Figure S3A)(Chen and Contreras, 2007; Janssens et al., 2015; Patterson and Maxwell, 2014). As expected, in wild-type cells Tom70-GFP and WGA intensity increased markedly from log phase to 24 hours and from 24 to 48 hours (Figure 3A, B). Cell size increased particularly during the first 24 hours of ageing (Figure 3C) while Rpl13a-mCherry increased only slightly (<1.5-fold, Figure S3B).

In *spt3*Δ, Tom70-GFP intensity increased with age to be significantly, although not substantially, lower than wild type at 24 hours, but did not increase from 24 to 48 hours despite cells reaching equivalent age to wild type (Figure 3A, B). *spt3*Δ cells were slightly smaller at all ages, but still grew substantially with age, while Rpl13a-mCherry intensity decreased with age though again the change was small (Figure 3C, S3B). Cells lacking Sac3 aged more slowly than wild type, reaching an average age in 48 hours only slightly higher than wild-type cells in 24 hours, but taking this into account behaved in a very similar manner to the *spt3*Δ mutant (Figure S3C). In contrast, *rad52*Δ cells showed significantly higher Tom70-GFP fluorescence than wild type at 24 hours, even though *rad52*Δ cells were younger, as well as being slightly though not significantly larger (Figure 3A, B). None of these

parameters changed from 24 to 48 hours consistent with *rad52*Δ cells reaching the end of replicative life before 24 hours, such that by 48 hours wild-type cells had caught up in Tom70-GFP and cell size. Taken together, we observe essentially no correlation between SEP onset or cell size and the accumulation of ERCs across this set of mutants.

We expanded on this surprising observation using epistasis assays, in which *rad52*Δ was combined with *spt3*Δ or *sac3*Δ. We expected that the high Tom70-GFP and low WGA phenotypes of the *rad52*Δ mutant would be dominant in these double mutants, as it seemed likely that whatever persistent DNA damage drives the SEP in *rad52*Δ cells should occur irrespective of SAGA or TREX-2 disruption. However, we actually observed a strong additive effect. One terminal phenotype of replicatively aged yeast, particularly in diploid MEP cell, is a cell division defect that causes <5% of cells to form large multicellular aggregates (Figure S3D). However, in the *rad52*Δ *spt3*Δ and *rad52*Δ *sac3*Δ double mutants, every mother cell formed such an aggregate within 24 hours, making purification impossible. This phenotype was prominent even in log phase populations (Figure 3D), and quantifying individual particles (a particle being 1 or more cells not separable by sonication) showed that the majority of double mutant cell particles were clusters of 3 or more cells, often containing 10+ cells (Figure 3D). This observation suggests that although *rad52*Δ mutants lack ERCs, *rad52*Δ mother cells may contain another toxic species that is normally retained in mother cells by SAGA / TREX-2.

The imaging data for *spt3*Δ and *sac3*Δ therefore show that ERC accumulation makes only a minor contribution to the SEP and *rad52*Δ develops a very strong SEP phenotype at a young age despite a complete absence of ERCs. Therefore, the presence or absence of ERCs does not define the SEP. Furthermore, the unexpected outcome of the epistasis assay raised the hypothesis that another DNA species is present in *rad52*Δ mutant cells, one that is normally retained in mother cells by SAGA and TREX-2 (just like ERCs) and which causes a cytokinesis defect if communicated to daughter cells.

A transcriptional signature of the SEP

The uncoupling of the SEP marker from ERC abundance prompted us to re-analyse our gene expression data looking for changes associated with the SEP. We defined another DESeq2 linear model with categorical independent variables for age, genotype and *TRP1* as before, but substituted the ERC level categorical variable for a continuous variable representing SEP status. This used Tom70-GFP intensity data for median values shown in Figure 3A and S3C scaled linearly from 0 to 1. The model discovered 187 genes significantly differentially expressed based on Tom70-GFP (DESeq2, BH-corrected FDR < 0.05, $\log_2$-fold change threshold ± 0.5), for which Tom70-GFP intensity was by far the strongest contributor to differential expression between datasets (Figure 4A, B). This means that differential expression of these genes was minimally affected by age or genotype in contrast to the previous model (compare Figure 4B to S2C). With this model we also found ~300 genes significantly differentially expressed based on age (DESeq2 48 hour vs. log phase age, BH-corrected FDR < 0.05, $\log_2$-fold change threshold ± 0.5), and age was by far the strongest model factor contributing to differential expression of these genes with little contribution from Tom70-GFP or genotype (Figure S4A, S4B).

GO analysis of the gene set differentially expressed based on Tom70-GFP revealed enrichments for sporulation, specifically genes for prospore formation, spore wall assembly and septins, as well as iron transport. In contrast, genes that increase with age are enriched for energy utilisation categories, reflecting the known changes in metabolism with age, while genes that decrease with age are associated with translation and ribosome synthesis. Therefore, gene expression changes that occur during ageing can be separated into those associated with the SEP and those associated with ageing itself.

One unexpected feature of the genes differentially expressed based on Tom70-GFP was that 22% are located on the right arm of chromosome XII between the rDNA and the telomere, a region

containing only 5% of annotated genes. This region, hereafter referred to as ChrXIIr, has been previously noted to be amplified during yeast ageing with unknown effect (Hu et al., 2014; Pal et al., 2018). We therefore asked whether the expression of genes in this region was generally disrupted in aged cells: indeed, average mRNA abundance for all genes on ChrXIIr increased with age in our wild type datasets (Figure 4C). Although many genes are induced with age, the average mRNA abundance change of any large, random set of genes between two datasets should be roughly zero due to the DESeq2 normalisation method applied. Indeed, an equivalent analysis for all genes not on chromosome XII shows no average change although the spread of mRNA abundance does increase with age as expected (Figure 4C right, S4C), so the effect on ChrXIIr is exceptional.

Increased mRNA abundance for ChrXIIr genes was much less evident in *spt3*Δ and almost undetectable in *sac3*Δ, despite an equivalent increase in the spread of mRNA abundance (Figure 4D, E compare grey to purple and orange). In contrast, average mRNA abundance for ChrXIIr genes dramatically increased in *rad52*Δ at 24 hours, significantly more so than in wild type (Figure 4D, E compare grey to green). Therefore, we observe two distinct gene expression signatures associated with the SEP: an increase in expression of spore wall and iron metabolism genes, and an average increase in mRNA abundance for genes on ChrXIIr, likely indicating amplification of this chromosomal region. These signatures are separable as the GO analysis and coefficient distribution for the genes differentially expressed based on Tom70-GFP is essentially identical if ChrXIIr genes are excluded (Figure S4D).

ChrXIIr rather than ERC accumulation is associated with the SEP

The increased expression of genes on ChrXIIr strongly suggested the accumulation of a chromosomal fragment from this region, as previously noted in aged wild-type cells (Hu et al., 2014; Pal et al., 2018). We therefore performed genome re-sequencing on DNA isolated from log, 24 hour and 48 hour-aged wild type, *spt3*Δ, *rad52*Δ and *sac3*Δ cells. The most dramatic change was rDNA copy number, which increased 14x with age in wild type due to ERC accumulation but not in the mutants (Figure 5A), however in *rad52*Δ cells the primary change with age was a 1.5-fold increase in ChrXIIr signal, equivalent to one additional copy of this region in these diploid cells (Figure 5B). ChrXIIr also accumulated in wild-type cells with age, but less so in *spt3*Δ and was almost undetectable in *sac3*Δ following very closely the pattern of Tom70-GFP fluorescence (compare Figure 5C to Figure 3A and S3C), while other chromosomes did not change on average (Figure 5C, right). Therefore, accumulation of an extra copy of ChrXIIr is robustly associated with the SEP.

We considered two potential mechanisms by which accumulation of such a non-centromeric fragment could contribute to the SEP. The dysregulation of gene expression caused by the imbalance in gene copy number could result in widespread defects in protein complement (Hose et al., 2020), or alternatively the presence of a large non-centromeric chromosomal fragment could itself impair the cell cycle. Of course, across the spectrum of age-linked pathology these explanations may not be mutually exclusive.

To determine whether dysregulation of the genes on ChrXIIr is associated with the SEP, we engineered a translocation in the MEP **a** haploid that relocated ChrXIIr to chromosome V and terminated chromosome XII with a telomere adjacent to the rDNA, forming the XIIr <> V strain (Figure 5D, S5A). For reasons that remain unclear, we were unable to generate this translocation in the α haploid and therefore the analysis was restricted to haploid cells, however mRNA-seq during ageing in wild-type haploid MEP cells detected a similar increase in abundance of ChrXIIr gene mRNAs to that observed in diploids (compare wild type Figure 5E to Figure 4D). In the XIIr <> V strain, ChrXIIr gene mRNAs did not increase in abundance with age, confirming that this effect arises through rDNA-induced chromosomal instability (Figure 5E). Nonetheless, the accumulation of Tom70-GFP with age and increasing cell size occurred just as in wild type, showing that although the SEP is associated with

formation of a chromosome XII fragment, the amplification of the specific set of genes on ChrXIIr is not causal (Figure 5F).

Overall, our results are entirely consistent with models that predict defects in rDNA stability to be potent drivers of ageing and age-linked phenotypes. However, we find no evidence that ERCs have a major impact on the physiology of aged cells *per se*; rather the formation of a non-centromeric fragment encompassing the region between the rDNA and the right telomere of chromosome XII is associated with the SEP as marked by Tom70-GFP fluorescence, and is a prime candidate for mediating many of the damaging effects of ageing in yeast.

Discussion

ERCs were first proposed as a cause of yeast ageing over 20 years ago, based on strong accumulation in short-lived mutants and the lifespan reduction caused by artificial ERCs (Sinclair and Guarente, 1997). However, the mechanism of ERC toxicity remains unknown and though recent studies linked defects in ribosome synthesis and nuclear pore structure to ERC accumulation, it is unclear whether or how these affect ageing cell physiology (Meinema et al., 2022; Morlot et al., 2019; Neurohr et al., 2018; Rempel et al., 2019). Here we examined ageing phenotypes in a panel of low-ERC mutants and found that age-associated transcriptomic dysregulation and the SEP occur essentially independently of ERCs. Furthermore, we did not find any robust indication of pathway specific impacts of ERCs at the transcriptional level. Thus, our data is incompatible with the hypothesis that ERCs are a primary driver of age-related changes in *S. cerevisiae,* and instead we identify another rDNA-derived extrachromosomal species that is tightly associated with the SEP.

A mechanism for ChrXIIr formation

Much of the evidence connecting ERCs to lifespan derives from mutations that increase or decrease ERC levels in young cells. However, these mutants are not absolutely specific and those that impact rDNA recombination will also affect the formation of other non-chromosomal DNA species including ChrXIIr. Many studies have attributed rDNA instability, ERC formation and reduced lifespan to replication fork stalling at the Fob1-mediated RFB, and SEP onset does not occur in ~70% of haploid *fob1*Δ cells (Benguria et al., 2003; Defossez et al., 1999; Johzuka and Horiuchi, 2002; Kaeberlein et al., 1999; Kobayashi et al., 1998; Kobayashi and Horiuchi, 1996; Morlot et al., 2019). If ChrXIIr causes the SEP, then formation must be promoted by Fob1. However, an alternative Fob1-independent pathway must also exist since ~30% of *fob1*Δ cells also undergo the SEP accompanied by strong ERC accumulation (Morlot et al., 2019). Given that we detect no difference in ERC abundance between aged wild type and *fob1*Δ, this Fob1-independent pathway may well be dominant in diploid MEP cells, so any mechanism for ChrXIIr formation must feature Fob1 but as a contributor rather than an indispensable component. Fob1 also promotes, but is not required for, loss of heterozygosity events at ChrXIIr that increase with age in diploid MEPs (Lindstrom et al., 2011).

Mechanistically, Fob1 blocks the passage of replication forks that would otherwise encounter the 35S RNA polymerase I transcription unit head-on (Figure 6A-ii), which are then resolved by replication forks travelling co-directionally with RNA polymerase I. However, if the co-directional fork becomes unrecoverably stalled then replication is not completed and a stable unreplicated structure would remain (Figure 6A-iii); indeed single-stranded rDNA intermediates have been directly observed to persist into anaphase in aged yeast (Neurohr et al., 2018). DNA replication in yeast can continue into anaphase, at which point this structure would become stretched between two mitotic spindles to form a bridging chromosome (Chan et al., 2009; Ivanova et al., 2020; Torres-Rosell et al., 2007) (Figure 6A-iv). The replication fork structures must then be cleaved by structure specific nucleases to allow completion of mitosis, as observed in mammalian systems (Chan et al., 2009; Chan et al., 2018; Naim et al., 2013; Ying et al., 2013), forming the ChrXIIr fragment as well as a truncated chromosome

XII (Figure 6A-v). Under this model, ChrXIIr forms through cleavage of replication intermediates that remain unresolved at anaphase, rather than through specific recombination events.

Replication fork stalling at the RFB does not occur in *fob1*Δ, but it is likely that replication head-on with RNA polymerase I would also cause unrecoverable fork stalling with the same outcome at a substantial frequency. Conversely, we predict that the frequency of unrecoverable stalling of replication forks in the rDNA would increase in a *rad52*Δ mutant as homologous recombination often rescues stalled replication forks (Ait Saada et al., 2018; Lambert et al., 2010), so ChrXIIr formation would occur more often and earlier during ageing in homologous recombination-deficient mutants. This would explain why the SEP phenotype is stronger in homologous recombination mutants than in wild type despite a complete lack of ERCs.

The ChrXIIr formation mechanism can also result in loss of heterozygosity in diploid cells (Figure 6B). If the in-tact chromosome XII segregates to the daughter after cleavage, the two cleaved chromosome XII fragments would remain in the mother cell to be repaired by single strand annealing in the next cell cycle (Figure 6B, left outcome)(Ozenberger and Roeder, 1991). However, if the centromeric fragment of the cleaved chromosome XII segregates to the daughter nucleus it becomes physically separated from the ChrXIIr fragment, which is not under tension and will be recruited to nuclear pores in the mother nucleus (Horigome et al., 2019). This results in loss of heterozygosity for the daughter cell, and ChrXIIr accumulation in the mother cell. Therefore, loss of heterozygosity events can be mechanistically linked to ChrXIIr formation and the SEP.

Resolving the ChrXIIr model with ageing cell genetics and physiology

Accumulation of the ChrXIIr fragment first reported by Hu *et al.* 2014 is likely to be affected by the vast majority of the mutants used to modulate ERC levels, though mechanistic dependencies for ChrXIIr and ERCs are not identical. Firstly, our ChrXIIr model resolves the long-standing issue of why homologous recombination mutants are short lived despite having no ERCs, since ChrXIIr formation should be accelerated in the absence of homologous recombination (Park et al., 1999). Secondly, the potent effects of replicative helicase mutants, particularly Sgs1, in accelerating ageing are readily understood under a model that invokes incomplete replication events in forming the pathological species (Sinclair and Guarente, 1997; Sinclair et al., 1997).

However, the widely reported impact of *sir2*Δ must be resolved. Sir2 silences RNA polymerase II activity in the otherwise highly transcribed intergenic spacer regions around the 5S gene (Figure 6A-i), so loss of Sir2 may impair progression of replication forks by increasing replication-transcription collisions (Garcia-Muse and Aguilera, 2016). Alternatively, rDNA silencing by Sir2 affects rDNA recombination in young cells through cohesin displacement; cohesin is lost from the rDNA during ageing and cohesin anchoring mutants undergo accelerated loss of heterozygosity with reduced lifespan, suggesting that aged cells are more sensitive to cohesin impairment (Chan et al., 2011; Kobayashi and Ganley, 2005; Lindstrom et al., 2011; Pal et al., 2018). Cohesin displacement is thought to directly affect rDNA recombination reactions by increasing freedom of broken chromosome ends, but the effect may be less direct in ageing cells as cohesin is involved in replication fork restart (Kobayashi et al., 2004; Tittel-Elmer et al., 2012; van Schie and de Lange, 2021). In other words, cohesin displacement would also increase unrecoverable replication fork stalling, increasing the frequency at which cells enter anaphase with incompletely replicated rDNA (Figure 6A).

The relationship between ERCs and ageing has been previously questioned by Ganley *et al.* who demonstrated that reducing the efficiency of rDNA replication origins decreased ERC abundance, but also decreased lifespan and rDNA stability (Ganley et al., 2009); we note that irrespective of the effect on ERCs, reducing origin efficiency would increase the chance that rDNA replication is not completed in a timely fashion and accelerate ChrXIIr formation. Overall, mutants that affect rDNA stability have phenotypes that are also coherent, or in some cases more coherent, with ChrXIIr rather

than ERCs as a driver of ageing. Similarly, the extended lifespan of mutants that fail to retain ERCs (Denoth-Lippuner et al., 2014; Shcheprova et al., 2008) and the transmission of senescence to daughter cells along with ERCs can be explained if ChrXIIr is retained by the same SAGA / TREX-2 dependent mechanism as ERCs (Neurohr et al., 2018). Nonetheless, it is clear that ChrXIIr and ERCs can only be mediators of specific pathology rather than primary drivers of ageing since mRNA dysregulation occurs essentially independent of ChrXIIr or ERCs and must respond to an underlying ageing process.

Our gene expression analysis revealed that an extra copy of ChrXIIr induces expression of spore wall synthesis and septin genes that are normally tightly repressed in vegetative growth. Spore wall structure and composition is very different from the normal cell wall, so mis-expression of spore wall components could easily impair cell wall structure to, for example, cause G1 arrest through the Cell Wall Integrity pathway (Kono et al., 2016). An effect of ChrXIIr through cell wall structure would be consistent with the unexpected *rad52*Δ *spt3*Δ and *rad52*Δ *sac3*Δ mutant phenotypes, as cell wall synthesis is separated between mother and daughter, and cell separation is controlled by the daughter nucleus (Bhavsar-Jog and Bi, 2017). So, while ChrXIIr retained in a mother cell would slow growth through cell wall dysfunction, ChrXIIr in the daughter could cause cell wall defects and may also impair cell separation, leading to the dramatic pseudohyphae-like cell aggregates that we observe.

The ERC model of yeast ageing has been remarkably effective in predicting and explaining yeast mutants with altered lifespans. However, these outcomes are difficult to translate to higher eukaryotes where evidence for ERC accumulation in ageing is lacking. Our findings show that other, lower copy number extrachromosomal DNA species are just as potent, if not more so, in mediating ageing phenotypes. Although we see essentially no correlation between ERCs and well-known age-related phenotypes, others have shown that synthetic ERCs can cause lifespan and nuclear pore defects, although rDNA sequences themselves are dispensable (Falcon and Aris, 2003; Meinema et al., 2022; Sinclair and Guarente, 1997). One parsimonious interpretation is that the critical parameter is the quantity of DNA associated with nuclear pores complexes irrespective of sequence. One ChrXIIr molecule (600 kb + rDNA) would then have the same impact as 70-250 monomeric ERCs (each of 9.1 kb) depending on where in the rDNA array the initial cleavage occurs, and so the SEP could be induced either by accumulation of a few ChrXIIr fragments or hundreds of ERCs, or a combination of both. Importantly, ChrXIIr-type non-centromeric fragments could arise through age-linked rDNA cleavage in higher eukaryotes but may have remained undetected due to their low copy number, raising the prospect of an rDNA stability mechanism of ageing that could be conserved from yeast to mammals.

Materials and Methods

Detailed and updated protocols are available at https://www.babraham.ac.uk/our-research/epigenetics/jon-houseley/protocols

Yeast culture and labelling

Yeast strains were constructed by standard methods and are listed in Table S1, oligonucleotide sequences are given in Table S2, plasmids in Table S3. For chromosome V <> XII translocation, Tom70-GFP was first tagged with GFP in MEP **a** using a variant of pFA6a-GFP-KanMX6 in which the I-*Sce*I site had been removed by site directed mutagenesis using oligos oJH1819-20, then *ade2*Δ was reverted by transforming with an *ADE2* fragment from BY4741. The Kan resistance gene in inducible I-*Sce*I plasmid pGSKU (Storici and Resnick, 2006) (*Sac*I-*Bmg*BI fragment) was replaced with the *TRP1* marker from pFA6a-TRP1 (Longtine et al., 1998) (*Sac*I-*Sma*I fragment) to form pGSTU. Then a 2 kb fragment of chromosome V with an I-*Sce*I site in the middle was inserted into pGSTU, using PCRs with oligos JH1798-9 (*Sac*I-*Bam*HI) and JH1800-1 (*Sac*II-*Bam*HI), and *Sac*I *Sac*II digested pGSTU to form pGST-V-U. The PCR product oJH1808-9 on this plasmid was transformed into Tom70-GFP *ADE2* haploid, colonies

were restreaked twice on YPGalactose plates before screening colonies by PCR for reciprocal transformations and confirmation by PFGE (0.5x TBE, 1% gel, 60-120s switching, 6 V/cm, 14 °C, 24 hours). The strain carrying the pJH1808-9 PCR product prior to streaking on galactose to induce the translocation was used as a control.

All cells were grown in YPD media (2% peptone, 1% yeast extract, 2% glucose) at 30°C with shaking at 200 rpm. Media components were purchased from Formedium and media was sterilised by filtration. MEP experiments were performed as described with modifications (Cruz et al., 2018): cells were inoculated in 4 ml YPx (where x is the sugar) and grown for 6-8 hours then diluted in 25 ml YPD and grown for 16-18 hours to 0.2-0.6x10^7 cells/ml in 50 ml Erlenmeyer flasks. 0.125x10^7 cells per aged culture were harvested by centrifugation (15 s at 13,000 g), washed twice with 125 µl PBS and re-suspended in 125 µl of PBS containing ~3 mg/ml Biotin-NHS (Pierce 10538723). Cells were incubated for 30 min on a wheel at room temperature, washed once with 125 µl PBS and re-suspended in 125 µl YPD then inoculated in 125 ml YPD at 1x10^4 cells/ml in a 250 ml Erlenmeyer flask (FisherBrand FB33132) sealed with Parafilm. 1 µM β-estradiol (from stock of 1 mM Sigma E2758 in ethanol) was added after 2 hours for wild type and *spt3*Δ, 3 hours for *sac3*Δ and 4 hours for *rad52*Δ. An additional 0.125x10^7 cells were harvested from the log phase culture while biotin labelling reactions were incubating at room temperature. Cells were harvested by centrifugation for 1 min, 4600 rpm, immediately fixed by resuspension in 70% ethanol and stored at -80°C. To minimise fluorophore bleaching during Tom70-GFP experiments, the window of the incubator was covered with aluminium foil, lights on the laminar flow hood were not used during labelling and tubes were covered with aluminium foil during biotin incubation.

Cell purification

Percoll gradients (1-2 per sample depending on harvest density) were formed by vortexing 900 µl Percoll (Sigma P1644) with 100 µl 10x PBS in 2 ml tubes and centrifuging 15 min at 15,000 g, 4 °C. Ethanol fixed cells were defrosted and washed with 1 volume of cold PBSE (PBS + 2 mM EDTA) before resuspension in ~100 µl cold PBSE per gradient and layering on top of the pre-formed gradients. Gradients were centrifuged for 4 min at 2,000 g, 4 °C, then the upper phase and brown layer of cell debris were removed and discarded. 1 ml PBSE was added, mixed by inversion and centrifuged 1 min at 2,000 g, 4 °C to pellet the cells, which were then re-suspended in 1 ml PBSE per time point (re-uniting samples that were split across two gradients). 25 µl Streptavidin microbeads (Miltenyi Biotech 1010007) were added and cells incubated for 5 min on a wheel at room temperature. Meanwhile, 1 LS column per sample (Miltenyi Biotech 1050236) was loaded on a QuadroMACS magnet and equilibrated with cold PBSE in a 4 °C room. Cells were loaded on columns and allowed to flow through under gravity, washed with 1 ml cold PBSE and eluted with 1 ml PBSE using plunger. Cells were re-loaded on the same columns after re-equilibration with ~500 µl PBSE, washed and re-eluted, and this process repeated for a total of three successive purifications. After addition of Triton X-100 to 0.01% to aid pelleting, cells were split into 2 fractions in 1.5 ml tubes, pelleted 30 s at 20,000 g, 4 °C, frozen on N2 and stored at -70 °C.

DNA extraction and Southern blot analysis

Cell pellets were re-suspended in 50 µl 0.34 U/ml lyticase (Sigma L4025) in 1.2 M sorbitol, 50 mM EDTA, 10 mM DTT and incubated at 37 °C for 45 min. After centrifugation at 1,000 g for 5 min, cells were gently re-suspended in 80 µl of 0.3% SDS, 50 mM EDTA, 250 µg/ml Proteinase K (Roche 3115801) and incubated at 65 °C for 30 min. 32 µl 5 M KOAc was added after cooling to room temperature, samples were mixed by flicking, and then chilled on ice for 30 min. After 10 min centrifugation at 20,000 g, the supernatant was extracted into a new tube using a cut tip, 125 µl phenol:chloroform pH 8 was added and samples were mixed on a wheel for 30 min. Samples were

centrifuged for 5 min at 20,000 g, the upper phase was extracted using cut tips, and precipitated with 250 µl ethanol. Pellets were washed with 70% ethanol, air-dried and left overnight at 4 °C to dissolve in 20 µl TE. After gentle mixing, 10 µl of each sample was digested with 20 U *Xho*I (NEB) for 3-6 hours in 20 µl 1x CutSmart buffer (NEB), 0.2 µl was quantified using PicoGreen DNA (Life Technologies), and equivalent amounts of DNA separated on 25 cm 1% 1x TBE gels overnight at 90 V. Gels were washed in 0.25 N HCl for 15 min, 0.5 N NaOH for 45 min, and twice in 1.5 M NaCl, 0.5 M Tris pH 7.5 for 20 min before being transferred to 20x20 cm HyBond N+ membrane in 6x SSC. Membranes were probed using random primed probes to the rDNA intergenic spacer region in 10 ml UltraHyb (Life Technologies) at 42 °C and washed with 0.1x SSC 0.1% SDS at 42 °C, or probed in Church Hyb at 65 °C and washed with 0.5x SSC 0.1% SDS at 65 °C. For probe synthesis, 25 ng template DNA in 38 µl water was denatured for 5 min at 95 °C, chilled on ice, then 10 µl 5x labelling buffer (5x NEBuffer 2, 25 µg/ml $d(N)_9$, 165 µM dATP, dGTP, dTTP), 1 µl Klenow exo- (NEB) and 0.2 µl 3000 Ci/mmol $\alpha[^{32}P]$-dCTP (at activity date, doubled every 2 weeks after up to 2.5 months) added before incubation for 1-3 hours at 37 °C, cleaning using a mini Quick Spin DNA column (Roche), and denaturing 5 min at 95 °C before adding to hybridisation buffer. Images were obtained by exposure to phosphorimaging screens (GE), developed using a FLA 7000 phosphorimager (GE) and quantified using ImageQuant v7.0 (GE). The Pulsed Field Gel in Figure S5 was run on a CHEF DRIII machine (Bio-Rad) using conditions: 0.5x TBE, 1% agarose, 60-120 s switch time , 6 V/cm, 14 °C, 24 hours run time, then blotted and probed as above using a random primed probe against the *BNA5* gene.

RNA extraction and RNA-seq library preparation

Cells were re-suspended in 50 µl Lysis/Binding Buffer (from mirVANA kit, Life Technologies AM1560), and 50 µl 0.5 µm zirconium beads (Thistle Scientific 11079105Z) added. Cells were lysed with 5 cycles of 30 s 6500 ms^{-1} / 30 s ice in an MP Fastprep bead beater or for 3 min at power 12 in a Bullet Blender (ThermoFisher) in cold room, then 250 µl Lysis/Binding buffer added followed by 15 µl miRNA Homogenate Additive and cells were briefly vortexed before incubating for 10 minutes on ice. 300 µl acid phenol : chloroform was added, vortexed and centrifuged 5 min at 13,000 g, room temperature before extraction of the upper phase. 400 µl room temperature ethanol and 2 µl glycogen (Sigma G1767) were added and mixture incubated for 1 hour at -30 °C before centrifugation for 15 minutes at 20,000 g, 4 °C. The pellet was washed with cold 70% ethanol and re-suspended in 10 µl water. 1 µl RNA was glyoxylated and analysed on a BPTE mini-gel, and RNA was quantified using a PicoGreen RNA kit (Life Technologies R11490) or Qubit® RNA HS Assay Kit.

150 ng RNA was used to prepare libraries using the NEBNext Ultra II Directional mRNAseq kit with poly(A)+ purification module (NEB E7760, E7490) as described with modifications: Reagent volumes for elution from poly(T) beads, reverse transcription, second strand synthesis, tailing and adaptor ligation were reduced by 50%; libraries were amplified for 13 cycles using 2 µl each primer per 50 µl reaction before two rounds of AMPure bead purification at 0.9x and elution in 11 µl 0.1x TE prior to quality control using a Bioanalyzer HS DNA ChIP (Agilent) and quantification using a KAPA Library Quantification Kit (Roche).

DNA extraction and library preparation for genome re-sequencing

Cells were resuspended in 60 µl PFGE wash buffer (10 mM Tris HCl pH 7.5, 50 mM EDTA) with 1 µl lyticase (17 U/ µl in 10 mM KPO_4 pH 7, 50% glycerol, Merck >2000 U/mg L2524), heated to 50°C for 2 min before addition of 40 µl molten CleanCut agarose (Bio-Rad 1703594), vortexing vigorously for 5 s before pipetting in plug mould (Bio-Rad 1703713) and solidifying 15-30 min at 4°C. Each plug was transferred to a 2 ml tube containing 500 µl PFGE wash buffer with 10 µl 17 U/µl lyticase and incubated 3 hours at 37°C. Solution was replaced with 500 µl PK buffer (100 mM EDTA pH 8, 0.2%

sodium deoxycholate, 1% sodium N-lauroyl sarcosine, 1 mg/ml Proteinase K) and incubated overnight at 50°C. Plugs were washed four times with 1 ml TE for 1-2 hours at room temperature with rocking, 10 mM PMSF was added to the second and third washes from 100 mM stock (Merck 93482). ½ plugs were equilibrated for 15 min with 1 ml agarase buffer (10 mM Bis-Tris-HCl, 1 mM EDTA pH 6.5), then the supernatant removed and 50 µl agarase buffer added. Plugs were melted for 20 min at 65°C, transferred for 5 min to a heating block pre-heated to 42°C, 1 µl β-agarase (NEB M0392S) was added and mixed by flicking without allowing sample to cool, and incubation continued at 42°C for 1 h. DNA was ethanol precipitated with 25 µl 10 M NH_4OAc, 1 µl GlycoBlue, 330 µl of ethanol and resuspended in 130 µl 0.1x TE. DNA was fragmented in an AFA microTUBE (Covaris 520045) in a Covaris E220 duty factor 10, PIP 175, Cycles 200, Temp 11°C, then ethanol precipitated. 10 ng DNA was used to prepare libraries using the NEBNext Ultra II DNA kit (NEB E7645S) as described with modifications: Reagent volumes for tailing and adaptor ligation were reduced by 75%; libraries were amplified for 9 cycles using 2 µl each primer per 50 µl reaction before two rounds of AMPure bead purification at 0.9x and elution in 11 µl 0.1x TE prior to quality control using a Bioanalyzer HS DNA ChIP (Agilent) and quantification using a KAPA Library Quantification Kit (Roche).

Sequencing

DNA- and RNA-seq libraries were sequenced by the Babraham Institute Sequencing Facility using a NextSeq 500 instrument on 75 bp single end mode. All RNA-seq data has been deposited at GEO under accession number GSE207429.

RNA-seq QC, mapping, quantification and analysis

FASTQ format files provided by the Babraham Institute Sequencing Facility were processed to integer read counts per gene using a Nextflow (v20.01.0) pipeline slightly modified from the RNA-seq pipeline provided by nf-core (v1.4.2)(Di Tommaso et al., 2017; Ewels et al., 2020). Reads were adapter and quality trimmed using Trim Galore! (v0.6.5) (www.bioinformatics.babraham.ac.uk/projects/trim_galore) wrapper around Cutadapt (v2.10) (Martin, 2011). Libraries were then assessed for overall quality using FastQC (v0.11.9) https://www.bioinformatics.babraham.ac.uk/projects/fastqc/. Reads were mapped to the R64-1-1 *S. cerevisiae* genome assembly using HISAT2 (v2.2.0) (Kim et al., 2015; Kim et al., 2019). Mapped reads were quantified over exons and grouped at the gene_id level using featureCounts (v2.0.0) (Liao et al., 2014). For mapping and quantification we used ENSEMBL release 99 annotation augmented with 4 additional loci between the canonical RNA Polymerase I-transcribed rRNA genes. The following were annotated with the "rDNA_intergenic" gene biotype: IGS2-1S at XII: 485433 - 459675, - strand; IGS2-1AS at XII: 458433 - 459675, + strand; IGS1-2S at XII: 459797 - 460711, - strand; IGS1-2AS at XII: 459797 - 460711, + strand. For downstream analyses we included all genes with annotated gene_biotype: "protein_coding", "transposable_element" or "rDNA_intergenic". We excluded all mitochondrially-encoded genes and those around the rDNA locus (i.e. with start or end positions within XII: 450000-491000) apart from ones with the "rDNA_intergenic" biotype. We performed most RNA-seq data manipulations downstream of featureCounts in the R (v4.2.1) programming environment (R Developer Core Team, 2022). We made significant use of the Tidyverse (v1.3.1) family of packages (Wickham et al., 2019), particularly stringr (v1.4.0), dplyr (v1.0.9), purrr (v0.3.4), tidyr (v1.2.0), readr (2.1.2) and tibble (v3.1.7). The DESeq2 (v1.36.0) (Love et al., 2014) package was obtained from the Bioconductor repository using BiocManager (v3.15)(Huber et al., 2015).

RNA-seq normalisation, differential expression testing and graphical output

In general, we used the built-in DESeq2 size factor normalisation process to make values comparable across sequenced libraries for visualisation as well as for differential expression testing. We applied a BH-corrected FDR cutoff of 0.05 for all differential expression tests. We categorised genes with $\log_2$ fold-change > 0.5 as significantly upregulated and genes with $\log_2$ fold-change < -0.5 as significantly downregulated. For display, we $\log_2$ transformed normalised read counts using an added pseudocount of 1 to deal with any instances of 0 detected counts.

The lists of significantly differentially expressed genes for Figures S1C and 2A were derived from a fitted DESeq2 model with Age (categorical, levels: log phase, 48 hours) as a single design factor. This included log phase and 48 hour aged samples in triplicate from the wild type background. Pairwise comparisons mentioned in section "ERC accumulation exerts minimal effects on individual genes" were performed using fitted DESeq2 models comparing 48 hour aged samples of wild type (triplicate) with *spt3*Δ (triplicate), *rad52*Δ (duplicate) or *sac3*Δ (triplicate) using Genotype (categorical, levels: wild type, mutant) as the single design factor.

Displayed data for Figure 2C as well as the list of genes displayed in heatmap 2B was derived from a fitted DESeq2 model with Age (categorical, levels: log phase, 24 hours, 48 hours), Genotype (categorical, levels: wild type, *spt3*Δ, *rad52*Δ and *sac3*Δ), ERC level (categorical, levels: low [i.e. most samples], high [i.e. wild type 24 hour and 48 hour samples]), and *TRP1* marker (categorical, levels: absent [wild type], present [all other genotypes]). This included log phase, 24 hour and 48 hour aged samples in triplicate for wild type, *TRP1*-repaired wild type, *spt3*Δ and *sac3*Δ as well as in duplicate for *rad52*Δ.

Displayed data for Figures 4B, 4C, 4D, 4E, S4A, S4B, S4C and S4D as well as the list of genes displayed in 4A and S4A was derived from a fitted DESeq2 model with Age (categorical, levels: log phase, 24 hours, 48 hours), Genotype (categorical, levels: wild type, *spt3*Δ, *rad52*Δ and *sac3*Δ), *TRP1* marker (categorical, levels: present [all apart from wild type], absent [wild type]) and TOM70-GFP (continuous, values taken from medians shown in Figure 3A and S3C min-max scaled to the range [0,1], wild type values also used for *TRP1*-repaired samples). For analysis of SIR complex-regulated genes, we considered genes to be regulated by the SIR complex if they were determined to be differentially expressed (under the original authors definition) in *sir2*Δ*, sir3*Δ and *sir4*Δ backgrounds by Ellahi *et al.* 2015 (bolded entries in Supplementary Table 7 from that publication). There were 40 of 42 genes present in our filtered RNA-seq dataset.

Displayed RNA-seq data for Figures 1C, 2B, 2D, 4A, S4A and 5E was adapter and quality trimmed using Trim Galore (v0.6.6) and was mapped to yeast genome R64-1-1 using HISAT2 v2.1.0 (Kim et al., 2019) by the Babraham Institute Bioinformatics Facility. Mapped data was imported into SeqMonk v1.47.0 (https://www.bioinformatics.babraham.ac.uk/projects/seqmonk/) and quantified for $\log_2$ total reads mapping to the antisense strand of annotated open reading frames (opposite strand specific libraries) with probes included to each strand of the rDNA intergenic spacer regions. Read counts were adjusted by Size Factor normalisation for the full set of quantified probes.

Hierarchical clustering plots and Principal Component Analyses were calculated within SeqMonk. MA plots were generated in GraphPad Prism (v9.2.0) comparing mean and difference for each gene between two conditions. Probes with less than 2 reads post normalisation in the control condition were filtered as change between datasets cannot be accurately quantified in this case.

Gene Ontology term enrichment analysis

GO analysis of individual clusters performed using GOrilla (http://cbl-gorilla.cs.technion.ac.il/) (Eden et al., 2009). Quoted p-values for GO analysis are FDR-corrected according to the Benjamini and Hochberg method (q-values from the GOrilla output). For brevity only the order of magnitude rather than the full q-value is given (Benjamini and Hochberg, 1995). Full GO analyses are provided in Supplementary File 1.

Genome re-sequencing mapping and analysis

After adapter and quality trimming using Trim Galore (v0.6.6), DNA-seq data was mapped to yeast genome R64-1-1 using Bowtie 2 (Langmead and Salzberg, 2012) by the Babraham Institute Bioinformatics Facility. Reads were quantified in 25 kb windows spaced every 5 kb. Windows overlapping Ty elements and LTRs, mitochondrial DNA, ENA locus and CUP1 locus were excluded then Size Factor normalisation applied (Anders and Huber, 2010). For rDNA analysis, reads were quantified in 1 kb windows, 200 bp spacing and Size Factor normalised.

Flow cytometry

Cell pellets were re-suspended in 240 µl PBS and 9 µl 10% triton X-100 containing 0.3 µl of 1 mg/ml Streptavidin conjugated with Alexa Fluor® 647 (Life technologies) and 0.6 µl of 1 mg/ml Wheat Germ Agglutinin (WGA) conjugated with CF®405S (Biotium). Cells were stained for 10 min at RT on a rotating mixer while covered with aluminium foil, washed once with 300 µl PBS containing 0.01% Triton X-100, re-suspended in 30 µl PBS and immediately subject to flow cytometry analysis. Flow cytometry analysis was conducted using an Amnis® ImageStream® X Mk II with the following laser power settings: 405=25mW, 488=180mW, 561=185mW, 642=5mW, SSC=0.3mW.

Cell populations were gated for single cells based on Area and Aspect Ratio (>0.8) values and in-focus cells were gated based on a Gradient RMS value (>50). Further gating of streptavidin positive (AF647) cells was also applied, all in a hierarchical manner and 1000 events acquired. Before data analysis, compensation was applied according to single-colour controls and a manual compensation matrix creation. Total fluorescence intensity values of different parameters were extracted using the Intensity feature of the IDEAS® software, with Adaptive Erode modified mask coverage. In the analysis, only positive values of fluorescence were included (i.e. where cells were truly positive for the marker) and median values of populations were determined with Graphpad Prism (v9.2.0).

Statistical analysis

All statistical analysis other than that performed using the R DESeq2 package was performed in GraphPad Prism (v9.2.0).

Acknowledgements

We would like to thank Rachael Walker and Attila Bebes of the Babraham Institute Flow Facility for their assistance with imaging flow cytometry, Paula Kokko-Gonzales and Nicole Forrester of the Babraham Institute Next Generation Sequencing facility for sequencing samples and QC assistance, and Felix Krueger, Laura Biggins and Anne Segonds-Pichon of the Babraham Institute Bioinformatics Facility for help with sample processing and statistical analysis. We thank Michelle King for southern blot analysis, Patrick Lindstrom and Dan Gottschling for the MEP system, Alex Whale, Gilles Charvin and Théo Aspert for helpful discussions, and Nianshu Zhang and Nazif Alic for helpful suggestions regarding DESeq2 linear modelling.

Funding

JH and AZ were funded by the Wellcome Trust [110216], AZ and DH by BBSRC DTP PhD awards [1645489, 1947502], JH and HHM by the BBSRC [BI Epigenetics ISP: BBS/E/B/000C0423], BP by Ecole Normale Superieure Paris-Saclay, Universite Paris-Saclay. The funders had no role in study design, data collection and analysis, decision to publish, or preparation of the manuscript.

This research was funded in whole, or in part, by the Wellcome Trust [Grant number 110216]. For the purpose of open access, the author has applied a CC BY public copyright licence to any Author Accepted Manuscript version arising from this submission.

References

Ait Saada, A., Lambert, S.A.E., and Carr, A.M. (2018). Preserving replication fork integrity and competence via the homologous recombination pathway. DNA Repair (Amst) *71*, 135-147.
Anders, S., and Huber, W. (2010). Differential expression analysis for sequence count data. Genome Biol *11*, R106.
Benguria, A., Hernandez, P., Krimer, D.B., and Schvartzman, J.B. (2003). Sir2p suppresses recombination of replication forks stalled at the replication fork barrier of ribosomal DNA in Saccharomyces cerevisiae. Nucleic Acids Res *31*, 893-898.
Bhavsar-Jog, Y.P., and Bi, E. (2017). Mechanics and regulation of cytokinesis in budding yeast. Seminars in cell & developmental biology *66*, 107-118.
Bryk, M., Briggs, S.D., Strahl, B.D., Curcio, M.J., Allis, C.D., and Winston, F. (2002). Evidence that Set1, a factor required for methylation of histone H3, regulates rDNA silencing in S. cerevisiae by a Sir2-independent mechanism. Curr Biol *12*, 165-170.
Chan, J.N., Poon, B.P., Salvi, J., Olsen, J.B., Emili, A., and Mekhail, K. (2011). Perinuclear cohibin complexes maintain replicative life span via roles at distinct silent chromatin domains. Dev Cell *20*, 867-879.
Chan, K.L., Palmai-Pallag, T., Ying, S., and Hickson, I.D. (2009). Replication stress induces sister-chromatid bridging at fragile site loci in mitosis. Nat Cell Biol *11*, 753-760.
Chan, Y.W., Fugger, K., and West, S.C. (2018). Unresolved recombination intermediates lead to ultra-fine anaphase bridges, chromosome breaks and aberrations. Nat Cell Biol *20*, 92-103.
Chen, C., and Contreras, R. (2007). Identifying genes that extend life span using a high-throughput screening system. Methods Mol Biol *371*, 237-248.
Cohen, S., Agmon, N., Sobol, O., and Segal, D. (2010). Extrachromosomal circles of satellite repeats and 5S ribosomal DNA in human cells. Mobile DNA *1*, 11.
Cohen, S., Yacobi, K., and Segal, D. (2003). Extrachromosomal circular DNA of tandemly repeated genomic sequences in Drosophila. Genome research *13*, 1133-1145.
Cruz, C., Della Rosa, M., Krueger, C., Gao, Q., Horkai, D., King, M., Field, L., and Houseley, J. (2018). Tri-methylation of histone H3 lysine 4 facilitates gene expression in ageing cells. eLife *7*, e34081.
Defossez, P.A., Prusty, R., Kaeberlein, M., Lin, S.J., Ferrigno, P., Silver, P.A., Keil, R.L., and Guarente, L. (1999). Elimination of replication block protein Fob1 extends the life span of yeast mother cells. Mol Cell *3*, 447-455.
Denoth-Lippuner, A., Krzyzanowski, M.K., Stober, C., and Barral, Y. (2014). Role of SAGA in the asymmetric segregation of DNA circles during yeast ageing. eLife *3*.
Di Tommaso, P., Chatzou, M., Floden, E.W., Barja, P.P., Palumbo, E., and Notredame, C. (2017). Nextflow enables reproducible computational workflows. Nat Biotechnol *35*, 316-319.
Ellahi, A., Thurtle, D.M., and Rine, J. (2015). The Chromatin and Transcriptional Landscape of Native Saccharomyces cerevisiae Telomeres and Subtelomeric Domains. Genetics *200*, 505-521.
Ewels, P.A., Peltzer, A., Fillinger, S., Patel, H., Alneberg, J., Wilm, A., Garcia, M.U., Di Tommaso, P., and Nahnsen, S. (2020). The nf-core framework for community-curated bioinformatics pipelines. Nat Biotechnol *38*, 276-278.
Falcon, A.A., and Aris, J.P. (2003). Plasmid accumulation reduces life span in Saccharomyces cerevisiae. J Biol Chem *278*, 41607-41617.
Fehrmann, S., Paoletti, C., Goulev, Y., Ungureanu, A., Aguilaniu, H., and Charvin, G. (2013). Aging yeast cells undergo a sharp entry into senescence unrelated to the loss of mitochondrial membrane potential. Cell reports *5*, 1589-1599.

Feser, J., Truong, D., Das, C., Carson, J.J., Kieft, J., Harkness, T., and Tyler, J.K. (2010). Elevated histone expression promotes life span extension. Mol Cell *39*, 724-735.
Ganley, A.R., Ide, S., Saka, K., and Kobayashi, T. (2009). The effect of replication initiation on gene amplification in the rDNA and its relationship to aging. Mol Cell *35*, 683-693.
Garcia-Muse, T., and Aguilera, A. (2016). Transcription-replication conflicts: how they occur and how they are resolved. Nat Rev Mol Cell Biol *17*, 553-563.
Gasch, A.P., Spellman, P.T., Kao, C.M., Carmel-Harel, O., Eisen, M.B., Storz, G., Botstein, D., and Brown, P.O. (2000). Genomic expression programs in the response of yeast cells to environmental changes. Molecular biology of the cell *11*, 4241-4257.
Ha, C.W., and Huh, W.K. (2011). Rapamycin increases rDNA stability by enhancing association of Sir2 with rDNA in Saccharomyces cerevisiae. Nucleic Acids Res *39*, 1336-1350.
Hallgren, J., Pietrzak, M., Rempala, G., Nelson, P.T., and Hetman, M. (2014). Neurodegeneration-associated instability of ribosomal DNA. Biochimica et biophysica acta *1842*, 860-868.
He, C., Zhou, C., and Kennedy, B.K. (2018). The yeast replicative aging model. Biochim Biophys Acta Mol Basis Dis *1864*, 2690-2696.
Hendrickson, D.G., Soifer, I., Wranik, B.J., Kim, G., Robles, M., Gibney, P.A., and McIsaac, R.S. (2018). A new experimental platform facilitates assessment of the transcriptional and chromatin landscapes of aging yeast. eLife *7*.
Horigome, C., Unozawa, E., Ooki, T., and Kobayashi, T. (2019). Ribosomal RNA gene repeats associate with the nuclear pore complex for maintenance after DNA damage. PLoS Genet *15*, e1008103.
Hose, J., Escalante, L.E., Clowers, K.J., Dutcher, H.A., Robinson, D., Bouriakov, V., Coon, J.J., Shishkova, E., and Gasch, A.P. (2020). The genetic basis of aneuploidy tolerance in wild yeast. eLife *9*.
Houseley, J., Kotovic, K., El Hage, A., and Tollervey, D. (2007). Trf4 targets ncRNAs from telomeric and rDNA spacer regions and functions in rDNA copy number control. EMBO J *26*, 4996-5006.
Houseley, J., and Tollervey, D. (2011). Repeat expansion in the budding yeast ribosomal DNA can occur independently of the canonical homologous recombination machinery. Nucleic Acids Res *39*, 8778-8791.
Hu, Z., Chen, K., Xia, Z., Chavez, M., Pal, S., Seol, J.H., Chen, C.C., Li, W., and Tyler, J.K. (2014). Nucleosome loss leads to global transcriptional up-regulation and genomic instability during yeast aging. Genes Dev *28*, 396-408.
Huber, W., Carey, V.J., Gentleman, R., Anders, S., Carlson, M., Carvalho, B.S., Bravo, H.C., Davis, S., Gatto, L., Girke, T., Gottardo, R., Hahne, F., Hansen, K.D., Irizarry, R.A., Lawrence, M., Love, M.I., MacDonald, J., Obenchain, V., Oles, A.K., Pages, H., Reyes, A., Shannon, P., Smyth, G.K., Tenenbaum, D., Waldron, L., and Morgan, M. (2015). Orchestrating high-throughput genomic analysis with Bioconductor. Nat Methods *12*, 115-121.
Hull, R.M., King, M., Pizza, G., Krueger, F., Vergara, X., and Houseley, J. (2019). Transcription-induced formation of extrachromosomal DNA during yeast ageing. PLoS Biol *17*, e3000471.
Ivanova, T., Maier, M., Missarova, A., Ziegler-Birling, C., Dam, M., Gomar-Alba, M., Carey, L.B., and Mendoza, M. (2020). Budding yeast complete DNA synthesis after chromosome segregation begins. Nature communications *11*, 2267.
Jack, C.V., Cruz, C., Hull, R.M., Keller, M.A., Ralser, M., and Houseley, J. (2015). Regulation of ribosomal DNA amplification by the TOR pathway. PNAS *112*, 9674-9679.
Janssens, G.E., Meinema, A.C., Gonzalez, J., Wolters, J.C., Schmidt, A., Guryev, V., Bischoff, R., Wit, E.C., Veenhoff, L.M., and Heinemann, M. (2015). Protein biogenesis machinery is a driver of replicative aging in yeast. eLife *4*, e08527.
Janssens, G.E., and Veenhoff, L.M. (2016a). Evidence for the hallmarks of human aging in replicatively aging yeast. Microb Cell *3*, 263-274.
Janssens, G.E., and Veenhoff, L.M. (2016b). The Natural Variation in Lifespans of Single Yeast Cells Is Related to Variation in Cell Size, Ribosomal Protein, and Division Time. PLoS One *11*, e0167394.
Johzuka, K., and Horiuchi, T. (2002). Replication fork block protein, Fob1, acts as an rDNA region specific recombinator in S. cerevisiae. Genes Cells *7*, 99-113.

Kaeberlein, M. (2010). Lessons on longevity from budding yeast. Nature *464*, 513-519.
Kaeberlein, M., McVey, M., and Guarente, L. (1999). The SIR2/3/4 complex and SIR2 alone promote longevity in Saccharomyces cerevisiae by two different mechanisms. Genes Dev *13*, 2570-2580.
Kim, D., Langmead, B., and Salzberg, S.L. (2015). HISAT: a fast spliced aligner with low memory requirements. Nat Methods *12*, 357-360.
Kim, D., Paggi, J.M., Park, C., Bennett, C., and Salzberg, S.L. (2019). Graph-based genome alignment and genotyping with HISAT2 and HISAT-genotype. Nat Biotechnol *37*, 907-915.
King, G.A., Goodman, J.S., Schick, J.G., Chetlapalli, K., Jorgens, D.M., McDonald, K.L., and Unal, E. (2019). Meiotic cellular rejuvenation is coupled to nuclear remodeling in budding yeast. eLife *8*.
Kobayashi, T., and Ganley, A.R. (2005). Recombination regulation by transcription-induced cohesin dissociation in rDNA repeats. Science *309*, 1581-1584.
Kobayashi, T., Heck, D.J., Nomura, M., and Horiuchi, T. (1998). Expansion and contraction of ribosomal DNA repeats in Saccharomyces cerevisiae: requirement of replication fork blocking (Fob1) protein and the role of RNA polymerase I. Genes Dev *12*, 3821-3830.
Kobayashi, T., and Horiuchi, T. (1996). A yeast gene product, Fob1 protein, required for both replication fork blocking and recombinational hotspot activities. Genes Cells *1*, 465-474.
Kobayashi, T., Horiuchi, T., Tongaonkar, P., Vu, L., and Nomura, M. (2004). SIR2 regulates recombination between different rDNA repeats, but not recombination within individual rRNA genes in yeast. Cell *117*, 441-453.
Kono, K., Al-Zain, A., Schroeder, L., Nakanishi, M., and Ikui, A.E. (2016). Plasma membrane/cell wall perturbation activates a novel cell cycle checkpoint during G1 in Saccharomyces cerevisiae. PNAS *113*, 6910-6915.
Lambert, S., Mizuno, K., Blaisonneau, J., Martineau, S., Chanet, R., Freon, K., Murray, J.M., Carr, A.M., and Baldacci, G. (2010). Homologous recombination restarts blocked replication forks at the expense of genome rearrangements by template exchange. Mol Cell *39*, 346-359.
Langmead, B., and Salzberg, S.L. (2012). Fast gapped-read alignment with Bowtie 2. Nat Methods *9*, 357-359.
Lesur, I., and Campbell, J.L. (2004). The transcriptome of prematurely aging yeast cells is similar to that of telomerase-deficient cells. Molecular biology of the cell *15*, 1297-1312.
Leupold, S., Hubmann, G., Litsios, A., Meinema, A.C., Takhaveev, V., Papagiannakis, A., Niebel, B., Janssens, G., Siegel, D., and Heinemann, M. (2019). Saccharomyces cerevisiae goes through distinct metabolic phases during its replicative lifespan. eLife *8*.
Li, C., Mueller, J.E., and Bryk, M. (2006). Sir2 represses endogenous polymerase II transcription units in the ribosomal DNA nontranscribed spacer. Molecular biology of the cell *17*, 3848-3859.
Liao, Y., Smyth, G.K., and Shi, W. (2014). featureCounts: an efficient general purpose program for assigning sequence reads to genomic features. Bioinformatics *30*, 923-930.
Lin, S.J., Defossez, P.A., and Guarente, L. (2000). Requirement of NAD and SIR2 for life-span extension by calorie restriction in Saccharomyces cerevisiae. Science *289*, 2126-2128.
Lindstrom, D.L., and Gottschling, D.E. (2009). The mother enrichment program: a genetic system for facile replicative life span analysis in Saccharomyces cerevisiae. Genetics *183*, 413-422.
Lindstrom, D.L., Leverich, C.K., Henderson, K.A., and Gottschling, D.E. (2011). Replicative age induces mitotic recombination in the ribosomal RNA gene cluster of Saccharomyces cerevisiae. PLoS Genet *7*, e1002015.
Longtine, M.S., McKenzie, A., 3rd, Demarini, D.J., Shah, N.G., Wach, A., Brachat, A., Philippsen, P., and Pringle, J.R. (1998). Additional modules for versatile and economical PCR-based gene deletion and modification in Saccharomyces cerevisiae. Yeast *14*, 953-961.
Love, M.I., Huber, W., and Anders, S. (2014). Moderated estimation of fold change and dispersion for RNA-seq data with DESeq2. Genome Biol *15*, 550.
Lu, K.L., Nelson, J.O., Watase, G.J., Warsinger-Pepe, N., and Yamashita, Y.M. (2018). Transgenerational dynamics of rDNA copy number in Drosophila male germline stem cells. eLife *7*.

Mansisidor, A., Molinar, T., Jr., Srivastava, P., Dartis, D.D., Pino Delgado, A., Blitzblau, H.G., Klein, H., and Hochwagen, A. (2018). Genomic Copy-Number Loss Is Rescued by Self-Limiting Production of DNA Circles. Mol Cell *72*, 583-593 e584.

Martin, M. (2011). Cutadapt removes adapter sequences from high-throughput sequencing reads. 2011 *17*, 3.

Meinema, A.C., Marzelliusardottir, A., Mirkovic, M., Aspert, T., Lee, S.S., Charvin, G., and Barral, Y. (2022). DNA circles promote yeast ageing in part through stimulating the reorganization of nuclear pore complexes. eLife *11*.

Moreno, D.F., Jenkins, K., Morlot, S., Charvin, G., Csikasz-Nagy, A., and Aldea, M. (2019). Proteostasis collapse, a hallmark of aging, hinders the chaperone-Start network and arrests cells in G1. eLife *8*.

Morlot, S., Song, J., Leger-Silvestre, I., Matifas, A., Gadal, O., and Charvin, G. (2019). Excessive rDNA Transcription Drives the Disruption in Nuclear Homeostasis during Entry into Senescence in Budding Yeast. Cell reports *28*, 408-422 e404.

Mortimer, R.K., and Johnston, J.R. (1959). Life span of individual yeast cells. Nature *183*, 1751-1752.

Naim, V., Wilhelm, T., Debatisse, M., and Rosselli, F. (2013). ERCC1 and MUS81-EME1 promote sister chromatid separation by processing late replication intermediates at common fragile sites during mitosis. Nat Cell Biol *15*, 1008-1015.

Neurohr, G.E., Terry, R.L., Lengefeld, J., Bonney, M., Brittingham, G.P., Moretto, F., Miettinen, T.P., Vaites, L.P., Soares, L.M., Paulo, J.A., Harper, J.W., Buratowski, S., Manalis, S., van Werven, F.J., Holt, L.J., and Amon, A. (2019). Excessive Cell Growth Causes Cytoplasm Dilution And Contributes to Senescence. Cell *176*, 1083-1097 e1018.

Neurohr, G.E., Terry, R.L., Sandikci, A., Zou, K., Li, H., and Amon, A. (2018). Deregulation of the G1/S-phase transition is the proximal cause of mortality in old yeast mother cells. Genes Dev *32*, 1075-1084.

Ozenberger, B.A., and Roeder, G.S. (1991). A unique pathway of double-strand break repair operates in tandemly repeated genes. Mol Cell Biol *11*, 1222-1231.

Pal, S., Postnikoff, S.D., Chavez, M., and Tyler, J.K. (2018). Impaired cohesion and homologous recombination during replicative aging in budding yeast. Sci Adv *4*, eaaq0236.

Park, P.U., Defossez, P.A., and Guarente, L. (1999). Effects of mutations in DNA repair genes on formation of ribosomal DNA circles and life span in Saccharomyces cerevisiae. Mol Cell Biol *19*, 3848-3856.

Patterson, M.N., and Maxwell, P.H. (2014). Combining magnetic sorting of mother cells and fluctuation tests to analyze genome instability during mitotic cell aging in Saccharomyces cerevisiae. Journal of visualized experiments : JoVE, e51850.

R Developer Core Team (2022). A language and environment for statistical computing (R Foundation for Statistical Computing, Vienna, Austria).

Rattray, A.J., Shafer, B.K., and Garfinkel, D.J. (2000). The Saccharomyces cerevisiae DNA recombination and repair functions of the RAD52 epistasis group inhibit Ty1 transposition. Genetics *154*, 543-556.

Rempel, I.L., Crane, M.M., Thaller, D.J., Mishra, A., Jansen, D.P., Janssens, G., Popken, P., Aksit, A., Kaeberlein, M., van der Giessen, E., Steen, A., Onck, P.R., Lusk, C.P., and Veenhoff, L.M. (2019). Age-dependent deterioration of nuclear pore assembly in mitotic cells decreases transport dynamics. eLife *8*.

Salvi, J.S., Chan, J.N., Pettigrew, C., Liu, T.T., Wu, J.D., and Mekhail, K. (2013). Enforcement of a lifespan-sustaining distribution of Sir2 between telomeres, mating-type loci, and rDNA repeats by Rif1. Aging cell *12*, 67-75.

Sarnoski, E.A., Song, R., Ertekin, E., Koonce, N., and Acar, M. (2018). Fundamental Characteristics of Single-Cell Aging in Diploid Yeast. iScience *7*, 96-109.

Shcheprova, Z., Baldi, S., Frei, S.B., Gonnet, G., and Barral, Y. (2008). A mechanism for asymmetric segregation of age during yeast budding. Nature *454*, 728-734.

Sinclair, D.A., and Guarente, L. (1997). Extrachromosomal rDNA circles--a cause of aging in yeast. Cell *91*, 1033-1042.

Sinclair, D.A., Mills, K., and Guarente, L. (1997). Accelerated aging and nucleolar fragmentation in yeast sgs1 mutants. Science *277*, 1313-1316.
Smith, J.S., and Boeke, J.D. (1997). An unusual form of transcriptional silencing in yeast ribosomal DNA. Genes Dev *11*, 241-254.
Storici, F., and Resnick, M.A. (2006). The delitto perfetto approach to in vivo site-directed mutagenesis and chromosome rearrangements with synthetic oligonucleotides in yeast. Methods Enzymol *409*, 329-345.
Stults, D.M., Killen, M.W., Pierce, H.H., and Pierce, A.J. (2008). Genomic architecture and inheritance of human ribosomal RNA gene clusters. Genome research *18*, 13-18.
Tittel-Elmer, M., Lengronne, A., Davidson, M.B., Bacal, J., Francois, P., Hohl, M., Petrini, J.H.J., Pasero, P., and Cobb, J.A. (2012). Cohesin association to replication sites depends on rad50 and promotes fork restart. Mol Cell *48*, 98-108.
Torres-Rosell, J., De Piccoli, G., Cordon-Preciado, V., Farmer, S., Jarmuz, A., Machin, F., Pasero, P., Lisby, M., Haber, J.E., and Aragon, L. (2007). Anaphase onset before complete DNA replication with intact checkpoint responses. Science *315*, 1411-1415.
Ünal, E., Kinde, B., and Amon, A. (2011). Gametogenesis eliminates age-induced cellular damage and resets life span in yeast. Science *332*, 1554-1557.
Valori, V., Tus, K., Laukaitis, C., Harris, D.T., LeBeau, L., and Maggert, K.A. (2020). Human rDNA copy number is unstable in metastatic breast cancers. Epigenetics : official journal of the DNA Methylation Society *15*, 85-106.
van Schie, J.J.M., and de Lange, J. (2021). The Interplay of Cohesin and the Replisome at Processive and Stressed DNA Replication Forks. Cells *10*.
Wang, M., and Lemos, B. (2017). Ribosomal DNA copy number amplification and loss in human cancers is linked to tumor genetic context, nucleolus activity, and proliferation. PLoS Genet *13*, e1006994.
Watada, E., Li, S., Hori, Y., Fujiki, K., Shirahige, K., Inada, T., and Kobayashi, T. (2020). Age-Dependent Ribosomal DNA Variations in Mice. Mol Cell Biol *40*.
Watson, A.T., Garcia, V., Bone, N., Carr, A.M., and Armstrong, J. (2008). Gene tagging and gene replacement using recombinase-mediated cassette exchange in Schizosaccharomyces pombe. Gene *407*, 63-74.
Wickham, H., Averick, M., Bryan, J., Chang, W., Mcgowan, L.D.A., François, R., Grolemund, G., Hayes, A., Henry, L., Hester, J., Kuhn, M., Pedersen, T.L., Miller, E., Bache, S.M., Müller, K., Ooms, J., Robinson, D., Seidel, D.P., Spinu, V., Takahashi, K., Vaughan, D., Wilke, C., Woo, K., and Yutani, H. (2019). Welcome to the Tidyverse. Journal of Open Source Software *4*, 1686.
Winston, F., Durbin, K.J., and Fink, G.R. (1984). The SPT3 gene is required for normal transcription of Ty elements in S. cerevisiae. Cell *39*, 675-682.
Xu, B., Li, H., Perry, J.M., Singh, V.P., Unruh, J., Yu, Z., Zakari, M., McDowell, W., Li, L., and Gerton, J.L. (2017). Ribosomal DNA copy number loss and sequence variation in cancer. PLoS Genet *13*, e1006771.
Ying, S., Minocherhomji, S., Chan, K.L., Palmai-Pallag, T., Chu, W.K., Wass, T., Mankouri, H.W., Liu, Y., and Hickson, I.D. (2013). MUS81 promotes common fragile site expression. Nat Cell Biol *15*, 1001-1007.
Yiu, G., McCord, A., Wise, A., Jindal, R., Hardee, J., Kuo, A., Shimogawa, M.Y., Cahoon, L., Wu, M., Kloke, J., Hardin, J., and Mays Hoopes, L.L. (2008). Pathways change in expression during replicative aging in Saccharomyces cerevisiae. The journals of gerontology Series A, Biological sciences and medical sciences *63*, 21-34.

Figures

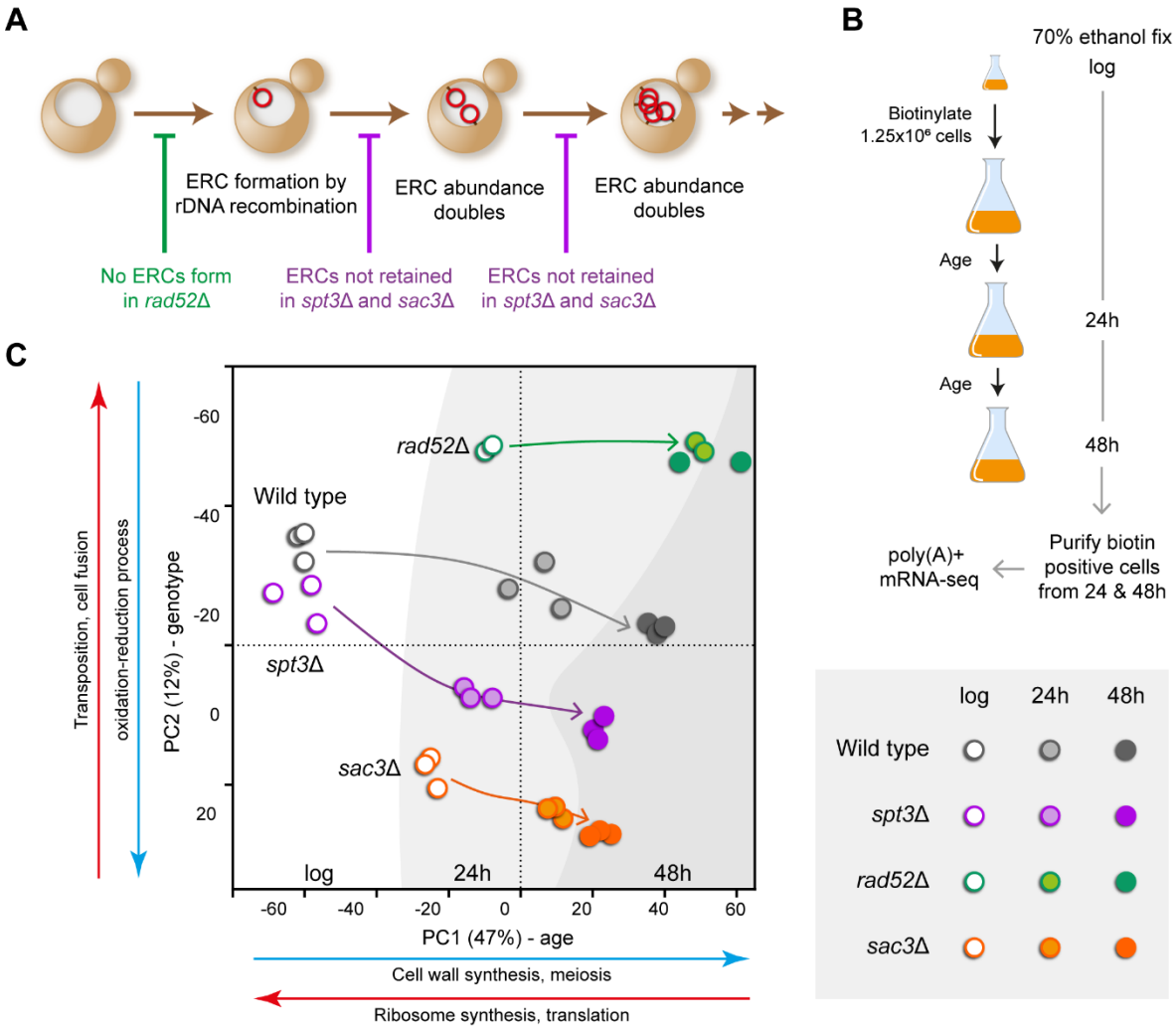

Figure 1: ERCs do not cause genome wide expression dysregulation

A: Schematic of ERC accumulation during replicative ageing, indicating the steps that are impaired in *rad52*Δ, *spt3*Δ and *sac3*Δ mutants.

B: Schematic of the mother enrichment programme (MEP) culture system used to isolate aged populations for analysis. Times of biotin labelling and harvest are shown.

C: Principal component analysis summary for young and aged poly(A)+ RNAseq libraries of wild type and indicated ERC mutants aged in YPD using the MEP. Arrows show progress of ageing, background colour graduations indicate age time point. Major GO categories for each PC are indicated based on the 300 highest rotation genes underlying the PC in either direction, full GO analysis in Supplementary File 1.

D: MA plots comparing $\log_2$ mRNA abundance distributions between log phase and 48 hour-aged samples from wild type and indicated mutants. X axis is $\log_2$ average normalised read count, Y axis is change in $\log_2$ normalised read count from young to old. Slope is calculated by linear regression. Data for each genotype and age calculated as the $\log_2$ mean normalised read counts per gene of 3 biological replicates for wild type, *spt3*Δ and *sac3*Δ or 2 biological replicates for *rad52*Δ.

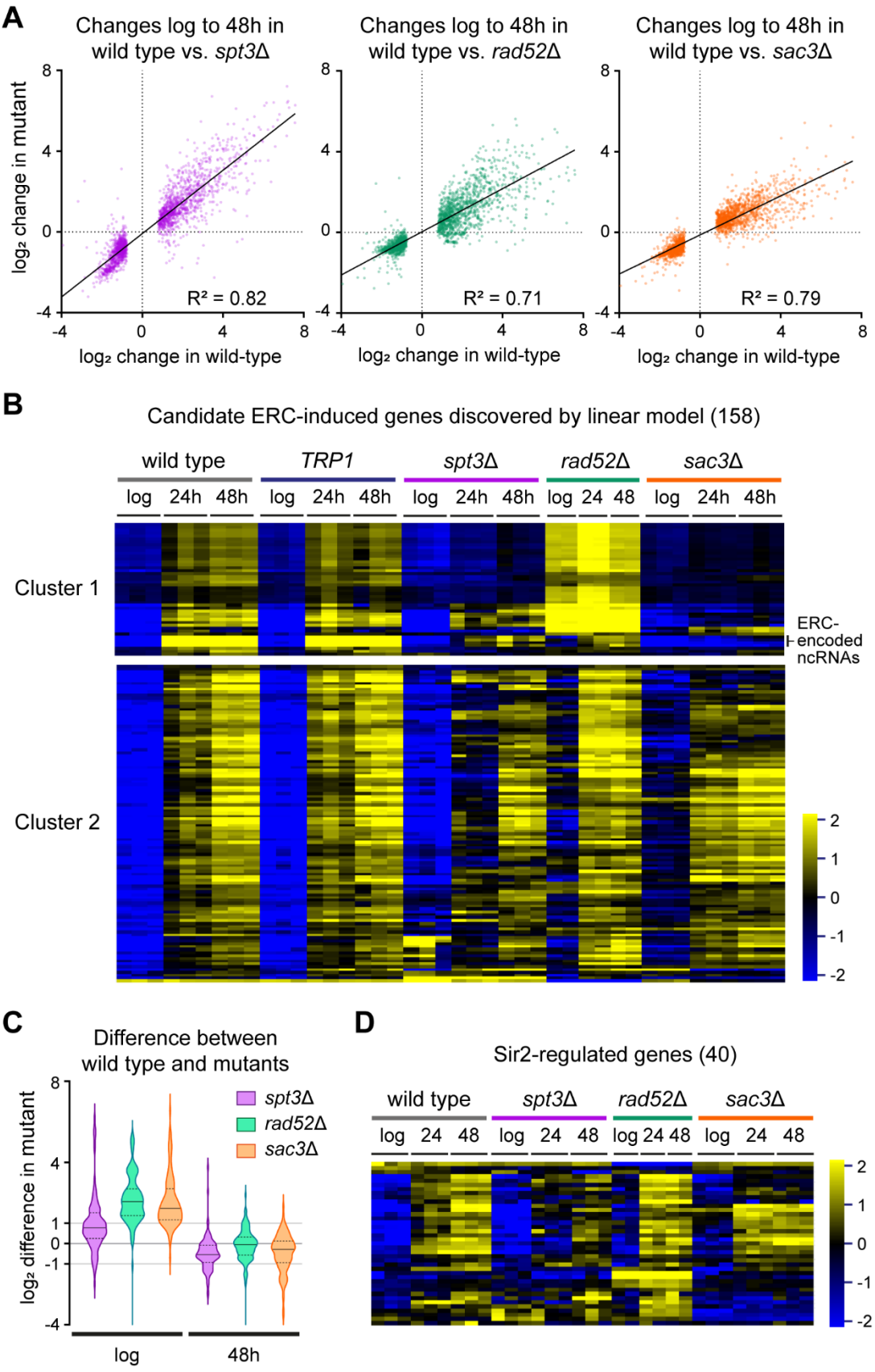

Figure 2: Expression charge of individual genes is not associated with ERC accumulation

A: Plots of change in $\log_2$ mRNA abundance between log phase and 48 hour-aged cells for each individual mutant compared to wild type. Only genes called as significantly differentially expressed with age in wild type (DESeq2 pairwise comparison of wild type 48 hour aged vs. log phase, Benjamini-Hochberg (BH) corrected false discovery rate (FDR) < 0.05, $\log_2$-fold change threshold ±0.5) are included. Slopes calculated by linear regression. Data for each genotype and age calculated as the $\log_2$ mean normalised read counts per gene of 3 biological replicates for wild type, *spt3*Δ and *sac3*Δ or 2 biological replicates for *rad52*Δ. Log_2 change calculated as the difference between $\log_2$ means for 48 hour and log phase samples within a genotype.

B: Heatmap with hierarchically clustered rows showing $\log_2$ normalised mRNA abundance for the 158 genes significantly differentially upregulated in the presence of ERCs (DESeq2 linear model factor 'high' ERC level vs. 'low' ERC level, BH corrected (FDR) < 0.05, $\log_2$-fold change threshold ±0.5). The colour scale indicates the $\log_2$ fold change relative to the per-gene median. Individual biological replicates shown (6 for wild type; 3 for *spt3*Δ and *sac3*Δ; 2 for *rad52*Δ). Wild type cells with *TRP1* gene repaired are included in addition to standard MEP wild type and are almost identical.

C: Violin plot for the difference in $\log_2$ mean normalised mRNA abundance between wild type and given mutants at log phase and after 48 hours of ageing for the cluster 2 genes shown in B. Solid horizontal lines within violins indicate median values while lower and upper quartiles are indicated by dotted horizontal lines.

D: Heatmap with hierarchically clustered rows showing $\log_2$ normalised mRNA abundances for the set of Sir2 -regulated genes defined by Ellahi *et al*. (Ellahi et al., 2015). Individual biological replicates shown (3 for wild type, *spt3*Δ and *sac3*Δ and 2 for *rad52*Δ). Clustering procedure and scale as in B.

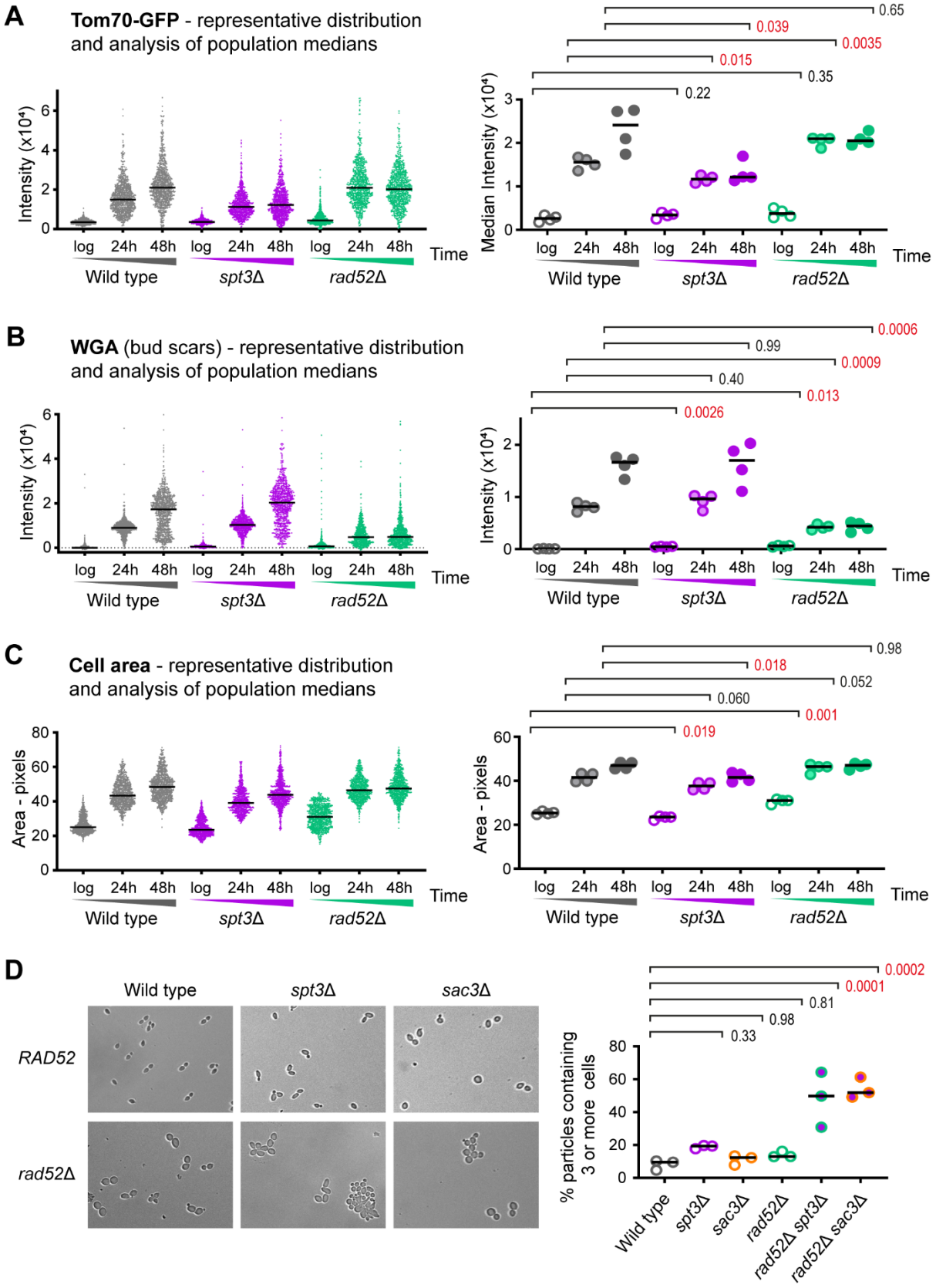

Figure 3: Mutants lacking ERCs still display signatures of the SEP

A: Imaging flow cytometry analysis of Tom70-GFP intensity, which increases hugely in G1 cells after the SEP (Fehrmann et al., 2013). Cells were gated for streptavidin staining (aged samples only) which filters out young cells, then for circularity which selects towards G1 cells and removes clumps. The left graph shows individual cells in a representative population with a bar at the median. The right graph compares medians of biological replicates. p values calculated from 2-way ANOVA with post-hoc Tukey test using genotype and age as independent variables, n=4. Red p values indicate significance at $p < 0.05$.

B: Analysis of WGA staining to show relative age. Samples and analysis as in A.

C: Analysis of cell size in pixels extracted from bright field images. Samples and analysis as in A.

D: Representative brightfield images of cells from log phase cultures of indicated genotypes. Samples were fixed in ethanol and sonicated to disperse cell clumps. Quantification shows the fraction of cell particles containing 3 or more cells (a particle being a unit of 1 or more cells that is not dispersed by sonication), analysis by one-way ANOVA with post-hoc Tukey test, n=3.

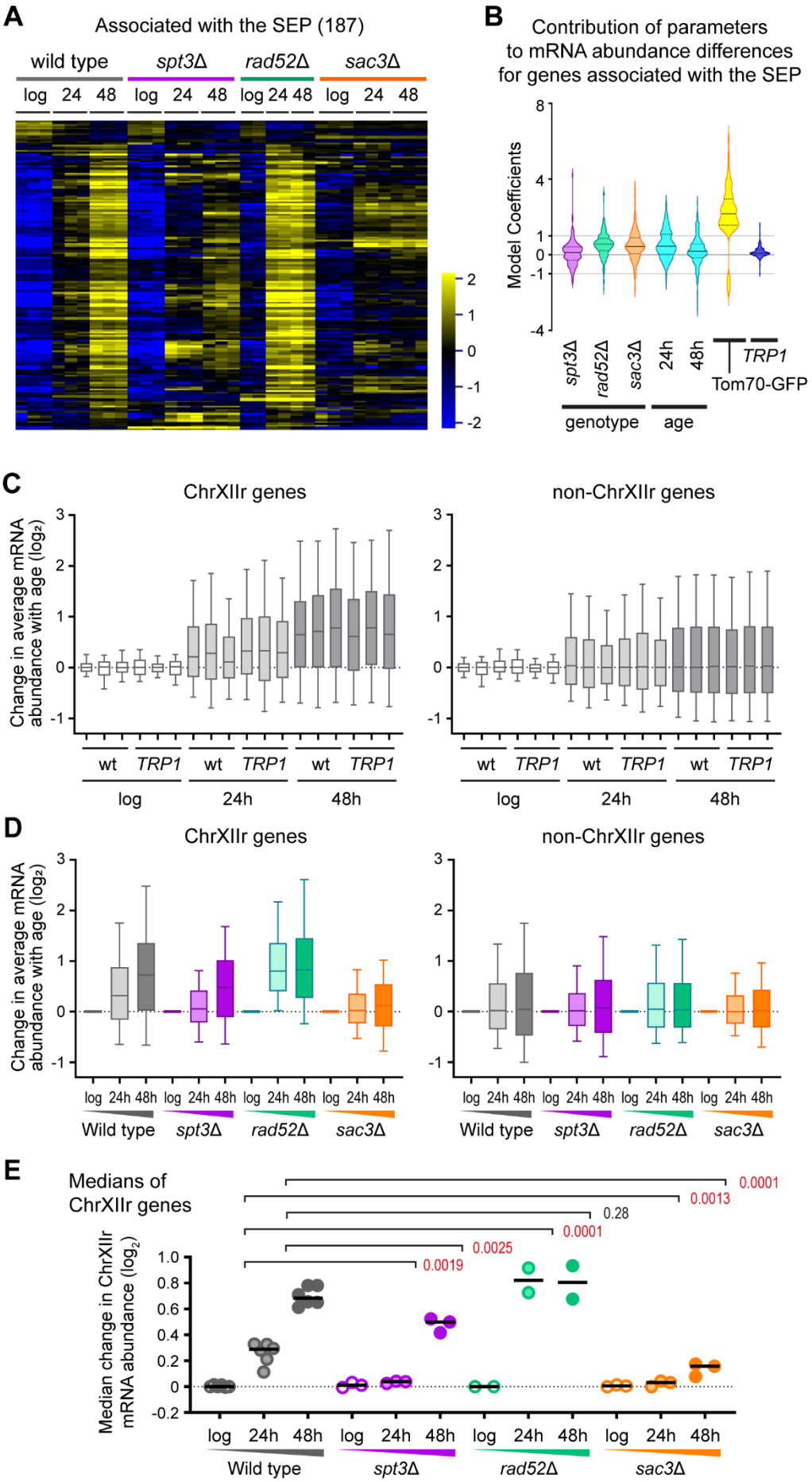

Figure 4: A gene expression signature for the SEP

A: Heatmap with hierarchically clustered rows of log_2 mRNA abundance for genes called by a DESeq2 linear model as significantly different between datasets based on the Tom70-GFP medians from Figure 3A and Figure S3C (DESeq2 continuous linear model factor: median Tom70-GFP scaled to between [0,1], BH-corrected FDR < 0.05, log_2-fold change threshold ±0.5). Individual biological replicates shown (3 for wild type, *spt3*Δ and *sac3*Δ and 2 for *rad52*Δ.

B: DESeq2 linear model coefficients representing the contribution of each individual parameter to the differences in mRNA abundance of the set of genes shown in A. DESeq2 was used to model expression as dependent on three categorical independent variables and one continuous variable (with an intercept factor not shown): Genotype (wild type, *spt3*Δ, *rad52*Δ, *sac3*Δ), *TRP1* auxotrophy (present, not present), Age (log phase, 24 hours, 48 hours), and Tom70-GFP (continuous, values taken from medians shown in Figure 3A and S3C min-max scaled to the range [0,1], wild type values also used for *TRP1*-repaired samples). Coefficient values can be interpreted as the log_2 normalised mRNA abundance change caused by a specific model factor being present relative to a wild type log phase *TRP1* auxotroph. Solid horizontal lines within violins indicate median values while lower and upper quartiles are indicated by dotted horizontal lines.

C: Log_2 change of mRNA abundance from log phase to given time points for all genes on ChrXIIr (left) or all genes on chromosomes other than XII (right). Individual biological replicates are shown, boxes show median and interquartile range, whiskers show upper and lower deciles.

D: Log_2 change of mRNA abundance from log phase to given time points for all genes on ChrXIIr (left) or all genes on chromosomes other than XII (right). Data is the mean of 3 biological replicates for wild type, *spt3*Δ and *sac3*Δ or 2 biological replicates for *rad52*Δ, plots as in C.

E. Analysis of median change in log_2 mRNA abundance from log phase to given time points for all genes on ChrXIIr. Analysis by two-way ANOVA with post-hoc Tukey test for aged time-points only since log values are the reference point n=6 biological replicates (wild type, combining wild type and *TRP1* datasets), n=3 for *spt3*Δ and *sac3*Δ, n=2 for *rad52*Δ. Red p values indicate significance at $p < 0.05$.

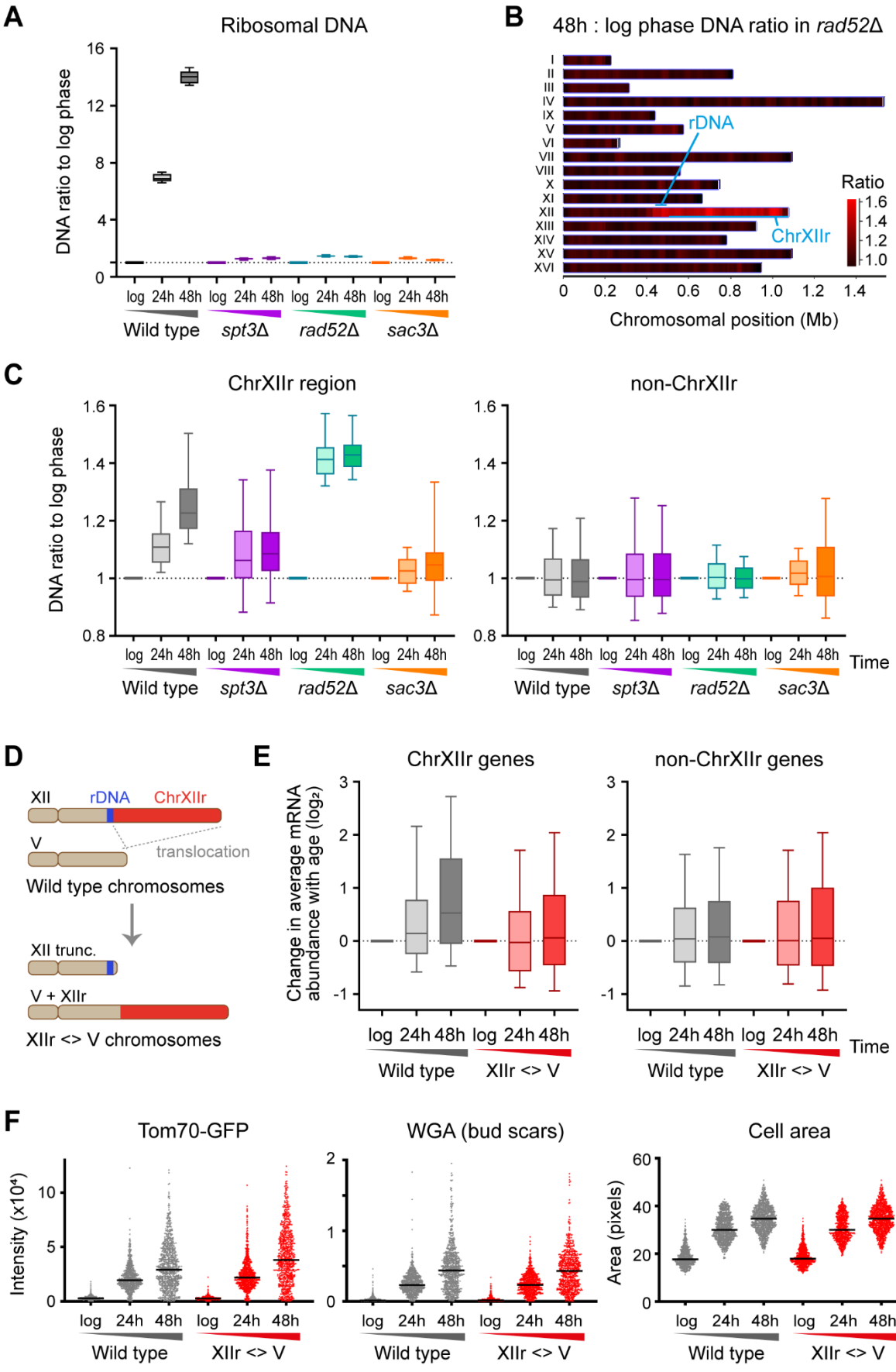

Figure 5: ChrXIIr amplification is associated with the SEP

A: Ratio of genome re-sequencing read counts at given time point to log phase in 5 kb windows across the rDNA.

B: Heat map of read count ratios between log phase and 48 hours in *rad52*Δ in 25 kb windows across the genome.

C: Ratio of genome re-sequencing read counts at given time point to log phase in 25 kb windows across ChrXIIr (left) and non-chromosome XII regions (right).

D: Schematic of translocation strategy for fusing ChrXIIr region to chromosome V.

E: Log_2 change of normalised mRNA abundance from log phase to given time points for all genes on ChrXIIr (left) or all genes on chromosomes other than XII (right). Both strains used are **a** haploids, the wild type contains the GST-V-U construct but translocation has not been induced.

F: Plots of Tom70-GFP and WGA intensity with cell size gated as in Figure 3 for wild type and chromosome XIIr <> V translocation strain, strains used are as in E.

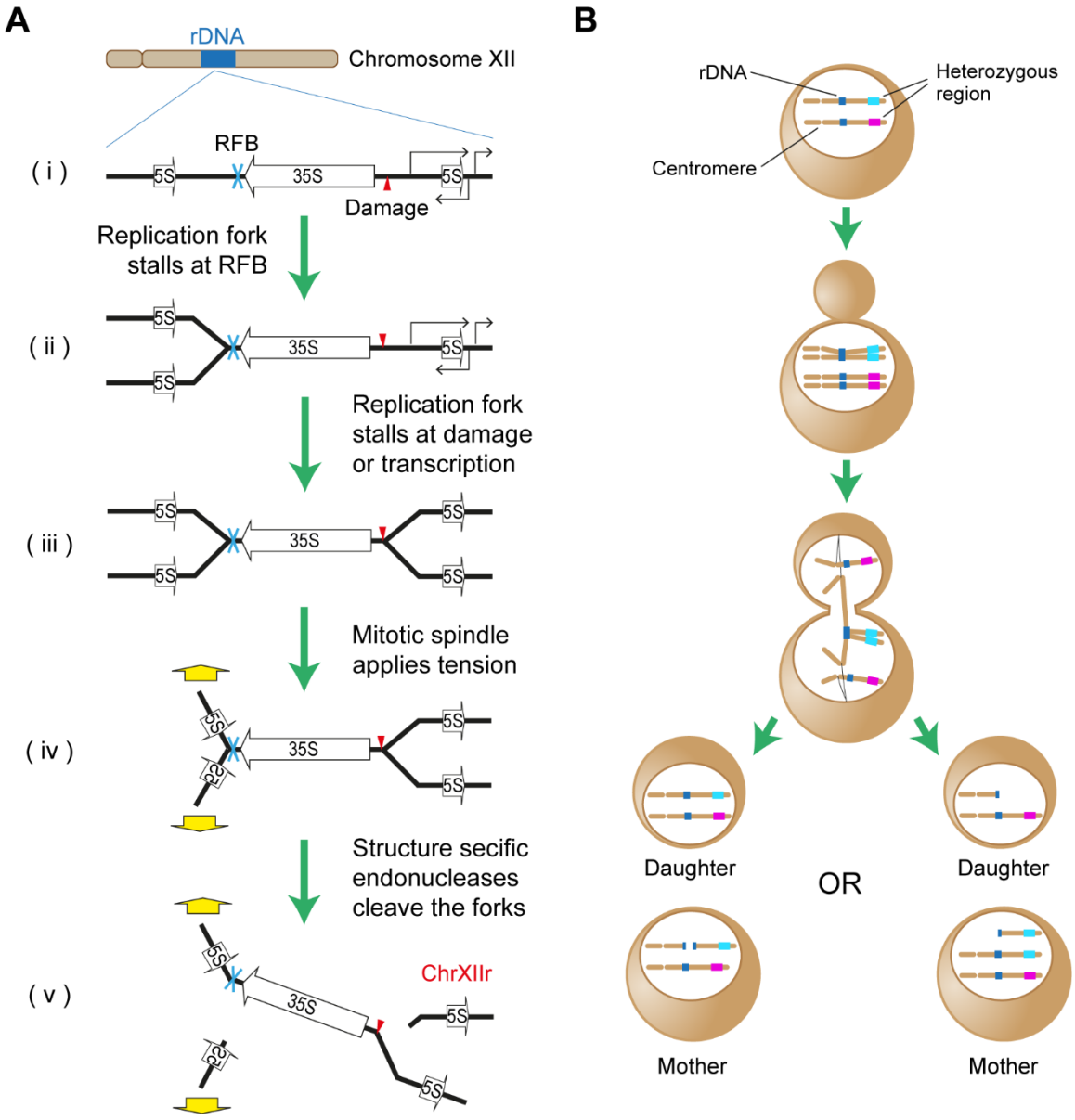

Figure 6: Model for the formation mechanism of ChrXIIr

A: Replication fork dynamics leading to incomplete replication at anaphase. (i) Potential replication fork stalling elements in the rDNA include the Replication Fork Barrier (RFB), DNA damage and regions highly expressed by RNA polymerase I, II and III. (ii) First replication fork stalls at the RFB or on collision with RNA polymerase I. (iii) Converging replication fork stalls due to DNA damage, collision with transcription units, topological strain, etc. (iv) Centromeres are pulled apart on the mitotic spindle, but segregation cannot be completed. (v) Cleavage of replication fork structures by structure specific endonucleases allows segregation to complete, but forms ChrXIIr.

B: ChrXIIr formation in the context of heterozygous markers. Incomplete replication leads to one chromosome forming a bridging chromosome, resolution of which either leaves both chromosome fragments in one nucleus (left), in which case the break can be repaired, or separates the fragments (right) in which case ChrXIIr formation in the mother is accompanied by loss of heterozygosity in the daughter. Further recombination events between ChrXIIr and full-length chromosome XII in the mother can lead to loss of heterozygosity also in the mother.

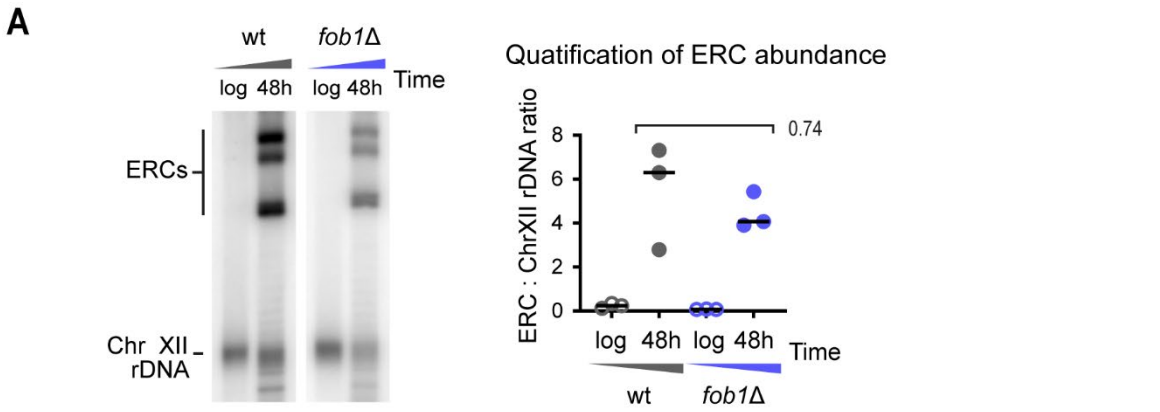

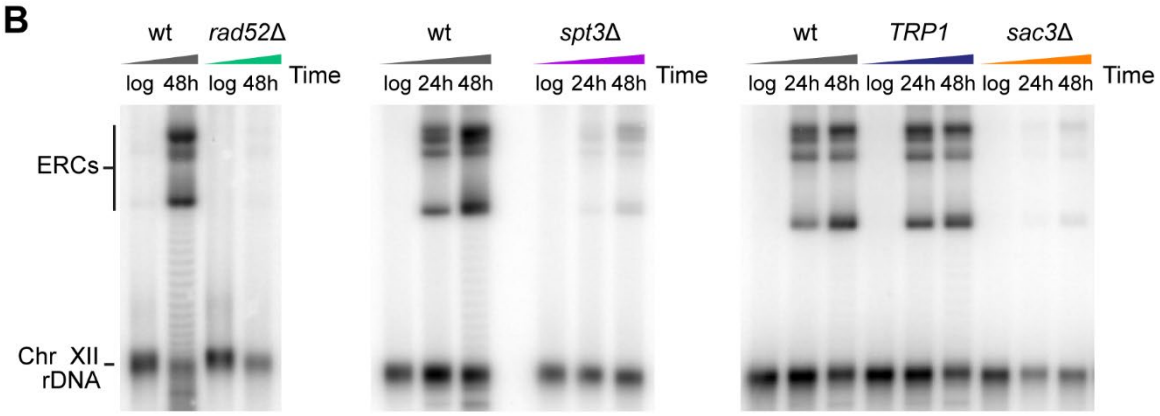

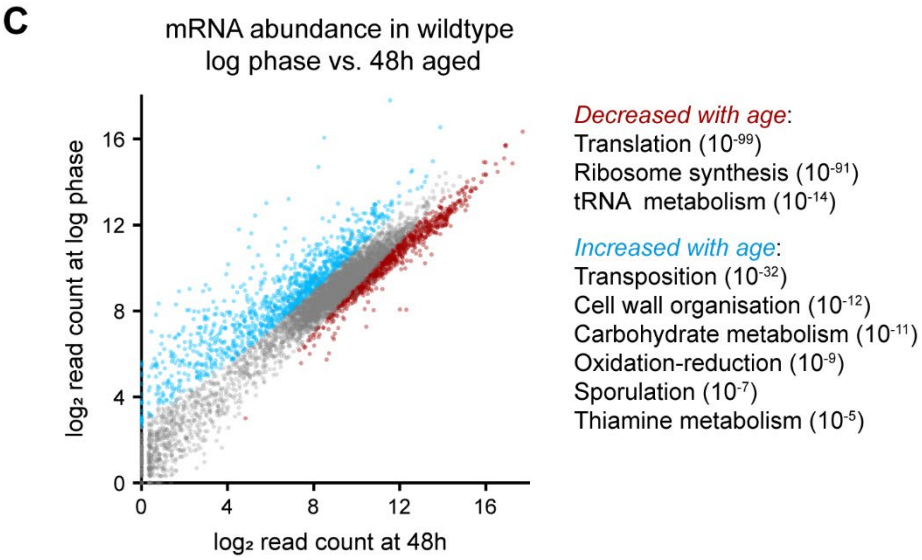

Figure S1: Supplement to ERCs do not cause genome wide expression dysregulation

A: Southern blot analysis of ERC abundance in log phase and 48 hour-aged wild-type and *fob1*Δ MEP cells. Quantification shows ratio between sum of ERC bands and chromosome XII band for 3 biological replicates, p value calculated by one-way ANOVA. Images show two sections of the same blot membrane with no differential image processing applied.

B: Southern blot analysis of ERC abundance at log phase and indicated aged timepoints for wild type, *rad52*Δ, *spt3*Δ and *sac3*Δ mutant MEP cells, along with a wild type in which the *TRP1* gene has been restored.

C: Scatter plot of $\log_2$ mRNA abundance comparing log phase to 48 hour-aged wild type, highlighting sets of genes called as significantly differentially expressed by DEseq2 (BH-corrected FDR<0.05, $\log_2$-fold change threshold ±0.5). GO terms are provided for each category, significance indicated by FDR-corrected q values, full GO analysis in Supplementary File 1.

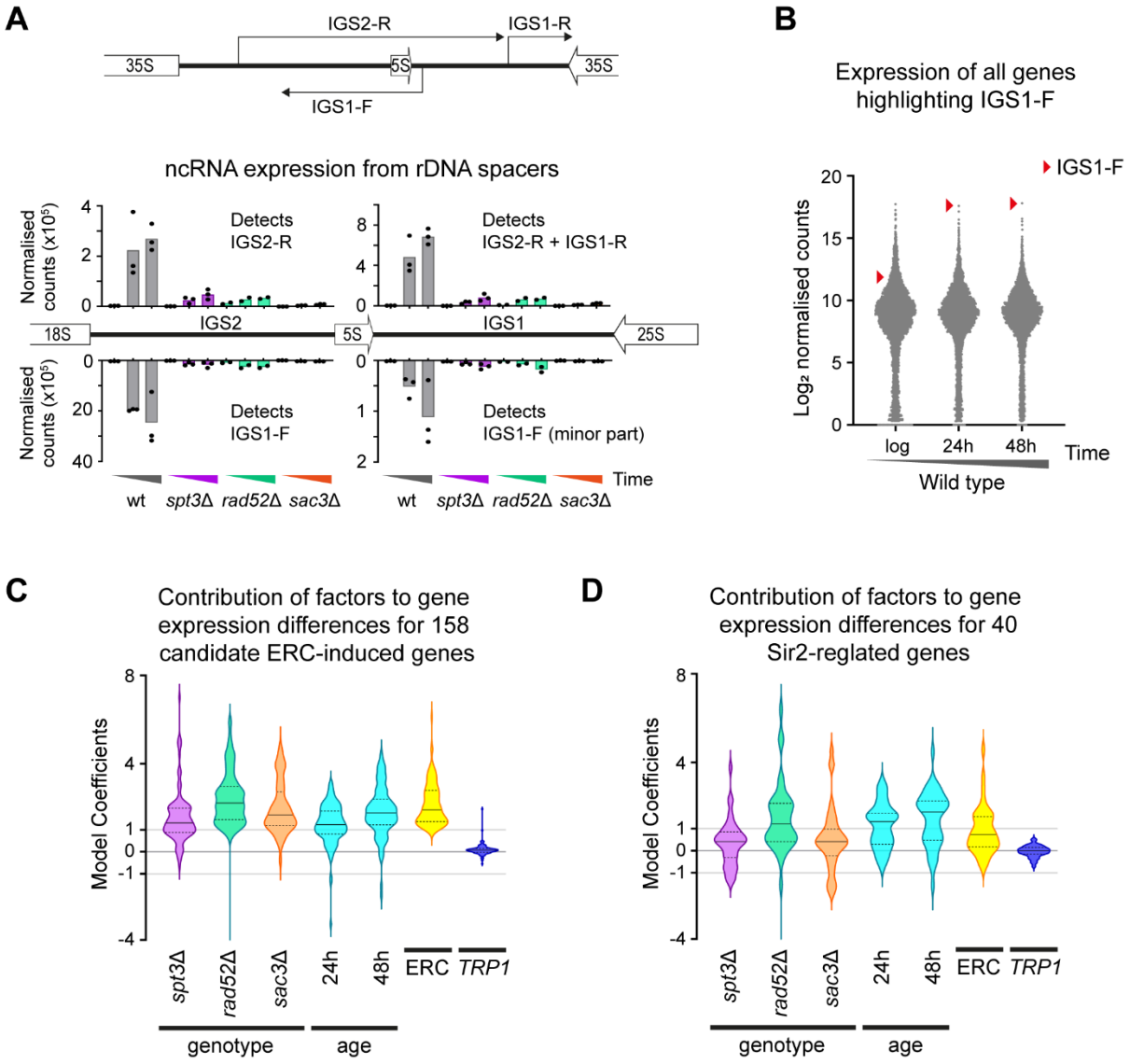

Figure S2: Supplement to expression charge of individual genes is not associated with ERC accumulation

A: Schematic of known RNA polymerase II transcripts in the intergenic spacer region of the rDNA, and quantification of non-coding transcripts orientated sense and antisense to the RNA polymerase I-transcribed 35S genes. Individual biological replicates are shown as points (3 for wild type, *spt3*Δ and *sac3*Δ and 2 for *rad52*Δ) and bars show mean values for a given age and genotype.

B: Distribution of $\log_2$ mean normalised mRNA abundance for all genes in wild-type cells including probes to rDNA intergenic spacer regions. Red arrows highlight the probe that detects the IGS1-F non-coding RNA as defined in panel A.

C: Coefficients representing the contribution of each individual DESeq2 linear model factor to mean $\log_2$ normalised mRNA abundance of cluster 2 genes (from Figure 2B) across all datasets. DESeq2 was used to model expression as dependent on four categorical independent variables (with an intercept factor not shown): Genotype (wild type, *spt3*Δ, *rad52*Δ, *sac3*Δ), *TRP1* auxotrophy (present, not present), Age (log phase, 24 hours, 48 hours), ERC accumulation (low, high). Coefficient values can be interpreted as the $\log_2$ normalised mRNA abundance change caused by a specific model factor being present relative to a wild type log phase *TRP1* auxotroph with low ERC levels. Solid horizontal lines within violins indicate median values while lower and upper quartiles are indicated by dotted horizontal lines.

D: As for C showing values for the 40 SIR-complex regulated genes (from Ellahi *et al.*) across all datasets.

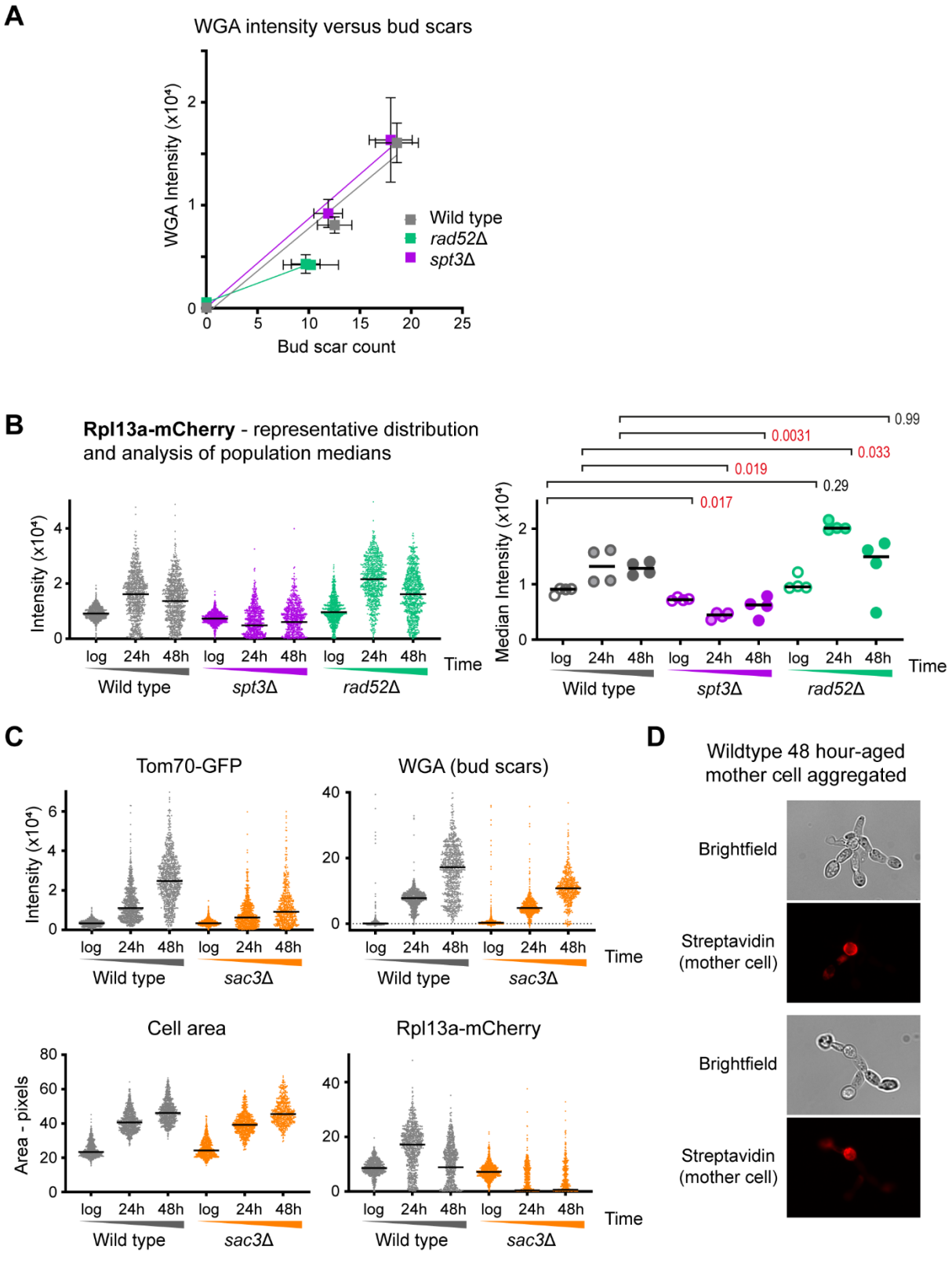

Figure S3: Supplement to mutants lacking ERCs still display signatures of the SEP

A: Comparison between manual bud scar counts and median WGA intensities for wild type, *spt3*Δ and *rad52*Δ at 24 and 48 hour time points. n=15 cells for bud scars, n=4 medians of biological replicate populations for WGA, error bars ±1 SD.

B: Analysis of Rpl13a-mCherry to show ribosomal protein abundance. Samples and analysis as in Figure 3A.

C: Plots of Tom70-GFP, Rpl13a-mCherry, WGA and cell size for wild-type and *sac3*Δ cells at indicated ages, obtained as in Figure 3A.

D: Example images of unseparated clusters of cells (brightfield) originating from single aged mother cells (streptavidin stained, red).

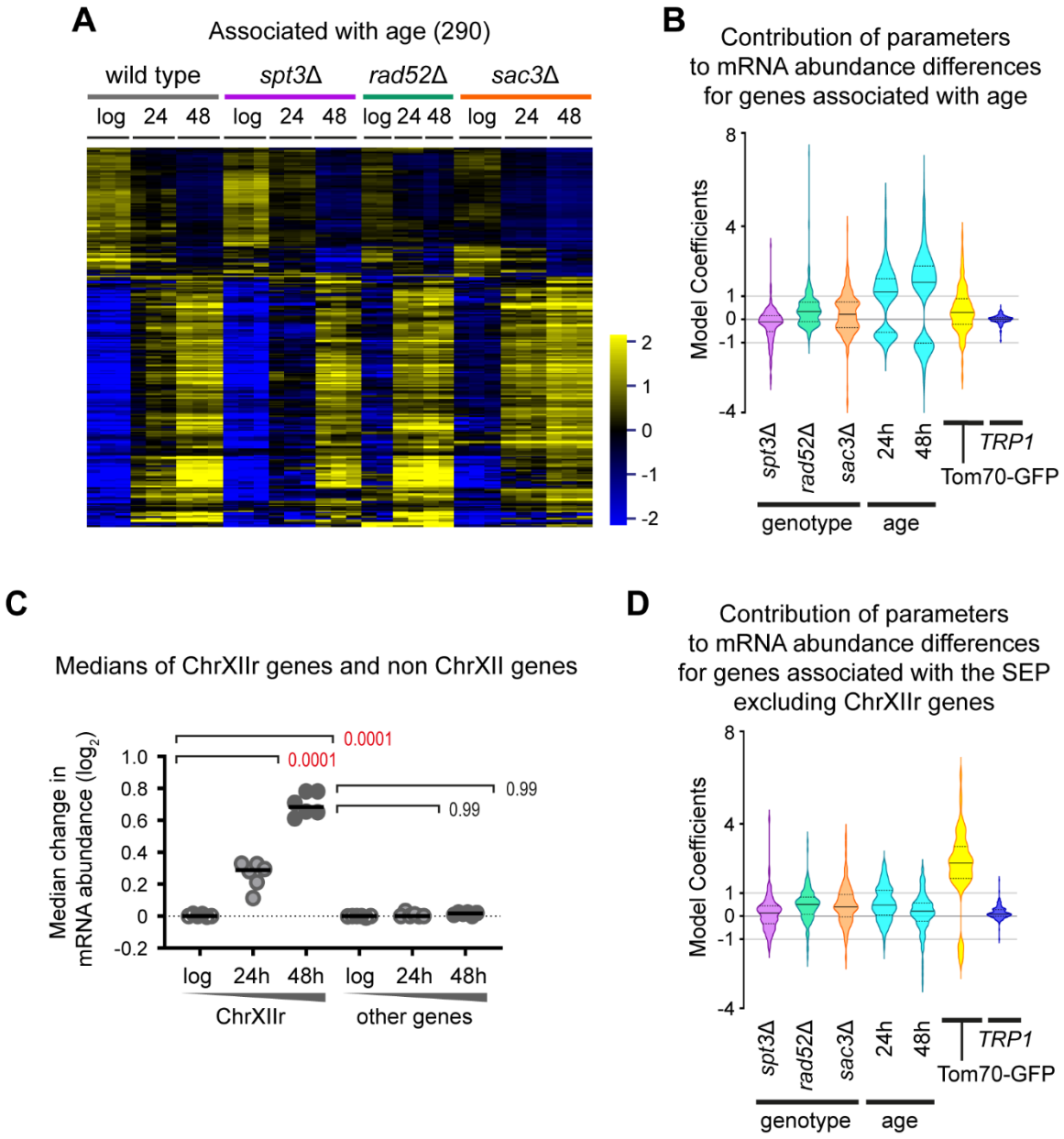

Figure S4: Supplement to a gene expression signature for the SEP

A: Heatmap with hierarchically clustered rows of $\log_2$ mRNA abundance for genes called by a DESeq2 linear model as significantly different between datasets based on age. DESeq2 modelling as described for 4B, clustering procedure as for 2B. Individual biological replicates shown (3 for wild type, *spt3*Δ and *sac3*Δ and 2 for *rad52*Δ).

B: Coefficients representing the contribution of each individual parameter to the differences in mRNA abundance of the set of genes significantly differentially expressed with Tom70-GFP levels across all datasets calculated using a DEseq2 linear model as described for 4B.

C: Medians of mRNA abundance change datasets (Figure 4C) for ChrXIIr and other chromosomes. Wild-type and TRP1 datasets are pooled to give n=6 per condition, p values calculated by one-way ANOVA with post-hoc Tukey test. Red p values indicate significance at $p < 0.05$.

D: As for B excluding genes on ChrXIIr.

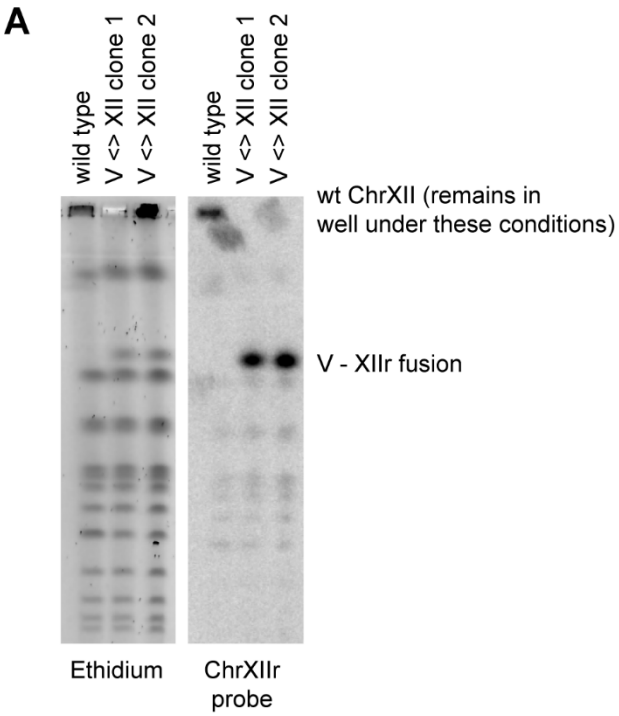

Figure S5: Supplement to ChrXIIr amplification is associated with the SEP

A: Pulsed field gel electrophoresis analysis showing successful translocation of ChrXIIr onto chromosome V.

YJH 1530	WT	*MAT a/MAT α ade2::hisG/ade2::hisG his3/his3 leu2/leu2 lys2/+ met15D::ADE2/+ ura3D0/ura3Δo trp1D63/trp1D63 hoD::SCW11pr-Cre-EBD78-NatMX/hoD::SCW11pr-Cre-EBD78-NatMX loxP-UBC9-loxP-LEU2/lOXp-UBC9-loxP-LEU2 loxP-CDC20-Intron-loxP-HPHMX/loxP-CDC20-Intron-loxP-HPHMX*	(Lindstrom and Gottschling, 2009)- UCC5185
YJH 1069	*spt3Δ*	*MAT a/MAT α ade2::hisG/ade2::hisG his3/his3 leu2/leu2 lys2/+ met15D::ADE2/+ ura3D0/ura3Δo trp1D63/trp1D63 hoD::SCW11pr-Cre-EBD78-NatMX/hoD::SCW11pr-Cre-EBD78-NatMX loxP-UBC9-loxP-LEU2/lOXp-UBC9-loxP-LEU2 loxP-CDC20-Intron-loxP-HPHMX/loxP-CDC20-Intron-loxP-HPHMX spt3::TRP1/spt3::TRP1*	(Hull et al., 2019)
YJH 1052	*rad52Δ*	*MAT a/MAT α ade2::hisG/ade2::hisG his3/his3 leu2/leu2 lys2/+ met15D::ADE2/+ ura3D0/ura3Δo trp1D63/trp1D63 hoD::SCW11pr-Cre-EBD78-NatMX/hoD::SCW11pr-Cre-EBD78-NatMX loxP-UBC9-loxP-LEU2/lOXp-UBC9-loxP-LEU2 loxP-CDC20-Intron-loxP-HPHMX/loxP-CDC20-Intron-loxP-HPHMX rad52::TRP1/rad52::TRP1*	This study
YAZ 47	*sac3Δ*	*MAT a/MAT α ade2::hisG/ade2::hisG his3/his3 leu2/leu2 lys2/+ met15D::ADE2/+ ura3D0/ura3Δo trp1D63/trp1D63 hoD::SCW11pr-Cre-EBD78-NatMX/hoD::SCW11pr-Cre-EBD78-NatMX loxP-UBC9-loxP-LEU2/lOXp-UBC9-loxP-LEU2 loxP-CDC20-Intron-loxP-HPHMX/loxP-CDC20-Intron-loxP-HPHMX sac3::TRP1/sac3::TRP1*	This study
YAZ 38	TRP1 repaired	*MAT a/MAT α ade2::hisG/ade2::hisG his3/his3 leu2/leu2 lys2/+ met15D::ADE2/+ ura3D0/ura3Δo hoD::SCW11pr-Cre-EBD78-NatMX/hoD::SCW11pr-Cre-EBD78-NatMX loxP-UBC9-loxP-LEU2/lOXp-UBC9-loxP-LEU2 loxP-CDC20-Intron-loxP-HPHMX/loxP-CDC20-Intron-loxP-HPHMX*	This study
YCJ 261	*fob1Δ*	*MAT a/MAT α ade2::hisG/ade2::hisG his3/his3 leu2/leu2 lys2/+ met15D::ADE2/+ ura3D0/ura3Δo trp1D63/trp1D63 hoD::SCW11pr-Cre-EBD78-NatMX/hoD::SCW11pr-Cre-EBD78-NatMX loxP-UBC9-loxP-LEU2/lOXp-UBC9-loxP-LEU2 loxP-CDC20-Intron-loxP-HPHMX/loxP-CDC20-Intron-loxP-HPHMX fob1Δ::kanMX.fob1Δ::kanMX*	(Lindstrom and Gottschling, 2009)- UCC526
YDH 57	spt3Δ TOM70-GFP Rpl13a-mCherry	*MAT a/MAT α ade2::hisG/ade2::hisG his3/his3 leu2/leu2 lys2/+ met15D::ADE2/+ ura3D0/ura3Δo trp1D63/trp1D63 hoD::SCW11pr-Cre-EBD78-NatMX/hoD::SCW11pr-Cre-EBD78-NatMX loxP-UBC9-loxP-LEU2/lOXp-UBC9-loxP-LEU2 loxP-CDC20-Intron-loxP-HPHMX/loxP-CDC20-Intron-loxP-HPHMX TOM70-GFP-TRP1/+ RPL13A-mCherry-KanMX6/+ spt3::URA3/spt3::URA3*	This study
YDH 52	rad52Δ TOM70-GFP Rpl13a-mCherry	*MAT a/MAT α ade2::hisG/ade2::hisG his3/his3 leu2/leu2 lys2/+ met15D::ADE2/+ ura3D0/ura3Δo trp1D63/trp1D63 hoD::SCW11pr-Cre-EBD78-NatMX/hoD::SCW11pr-Cre-EBD78-NatMX loxP-UBC9-loxP-LEU2/lOXp-UBC9-loxP-LEU2 loxP-CDC20-Intron-loxP-HPHMX/loxP-CDC20-Intron-loxP-HPHMX TOM70-GFP-TRP1/+ RPL13A-mCherry-KanMX6/+ rad52::URA3/rad52::URA3*	This study
YDH 18	TOM70-GFP Rpl13a-mCherry	*MAT a/MAT α ade2::hisG/ade2::hisG his3/his3 leu2/leu2 lys2/+ met15D::ADE2/+ ura3D0/ura3Δo trp1D63/trp1D63 hoD::SCW11pr-Cre-EBD78-NatMX/hoD::SCW11pr-Cre-EBD78-NatMX loxP-UBC9-loxP-LEU2/lOXp-UBC9-loxP-LEU2 loxP-CDC20-Intron-loxP-HPHMX/loxP-CDC20-Intron-loxP-HPHMX TOM70-GFP-TRP1/+ RPL13A-mCherry-KanMX6/+*	Horkai & Houseley 2021
YJH 1521	sac3Δ TOM70-GFP Rpl13a-mCherry	*MAT a/MAT α ade2::hisG/ade2::hisG his3/his3 leu2/leu2 lys2/+ met15D::ADE2/+ ura3D0/ura3Δo trp1D63/trp1D63 hoD::SCW11pr-Cre-EBD78-NatMX/hoD::SCW11pr-Cre-EBD78-NatMX loxP-UBC9-loxP-LEU2/lOXp-UBC9-loxP-LEU2 loxP-CDC20-Intron-loxP-HPHMX/loxP-CDC20-Intron-loxP-HPHMX TOM70-GFP-TRP1/+ RPL13A-mCherry-KanMX6/+ sac3::URA3/sac3::TRP1*	This study
YJH 1540	sac3Δ rad52Δ TOM70-GFP Rpl13a-mCherry	*MAT a/MAT α ade2::hisG/ade2::hisG his3/his3 leu2/leu2 lys2/+ met15D::ADE2/+ ura3D0/ura3Δo trp1D63/trp1D63 hoD::SCW11pr-Cre-EBD78-NatMX/hoD::SCW11pr-Cre-EBD78-NatMX loxP-UBC9-loxP-LEU2/lOXp-UBC9-loxP-LEU2 loxP-CDC20-Intron-loxP-HPHMX/loxP-CDC20-Intron-loxP-HPHMX TOM70-GFP-TRP1/+ RPL13A-mCherry-KanMX6/+ sac3::URA3/sac3::TRP1 rad52:HIS3/rad52::HIS3*	This study
YJH 1526	spt3Δ rad52Δ TOM70-GFP Rpl13a-mCherry	*MAT a/MAT α ade2::hisG/ade2::hisG his3/his3 leu2/leu2 lys2/+ met15D::ADE2/+ ura3D0/ura3Δo trp1D63/trp1D63 hoD::SCW11pr-Cre-EBD78-NatMX/hoD::SCW11pr-Cre-EBD78-NatMX loxP-UBC9-loxP-LEU2/lOXp-UBC9-loxP-LEU2 loxP-CDC20-Intron-loxP-HPHMX/loxP-CDC20-Intron-loxP-HPHMX TOM70-GFP-TRP1/+ RPL13A-mCherry-KanMX6/+ spt3::URA3/spt3::TRP1 rad52:HIS3/rad52::HIS3*	This study

YJH 1584	Tom70-GFP ADE2 GST-V-U	*MAT a his3 leu2 lys2 ura3DO trp1D63 hoD::SCW11pr-Cre-EBD78-NatMX loxP-UBC9-loxP-LEU2 loxP-CDC20-Intron-loxP-HPHMX Tom70-GFP-[no I-SceI]-KanMX6 chrXII:491k-pGST-chrVfrag-ISceIsite-chrVfrag-U*	This study
YJH 1594	Tom70-GFP ADE2 XII<>V translocation	*MAT a his3 leu2 lys2 ura3DO trp1D63 hoD::SCW11pr-Cre-EBD78-NatMX loxP-UBC9-loxP-LEU2 loxP-CDC20-Intron-loxP-HPHMX Tom70-GFP-[no I-SceI]-KanMX6 chrXII:1-491k-Pgal-SceI-TRP1--chrV:565k-end, chrV:1-565k--URA3-chrXII:491k-end*	This study

Table S1: Strains used in this work

All strains are in the MEP background, most are diploid as indicated. Wild-type alleles are indicated as +, TOM70 and RPL13a tagging constructs are heterozygous to avoid growth defects.

oJH1352	SPT3 UP45	GTGCATACAAGGTACCGTGCCAAAATTCAAGAGATTAGGGCAGGA CGGATCCCCGGGTTAATTAAG
oJH1353	SPT3 DN45	CCAGAAGGAAACCCATGCACCTCCATGATGAAATTATACAAAAAT GAATTCGAGCTCGTTTAAAC
oJH1354	SPT3 C	ACCCCATGATGATGTGATTG
oJH1355	SPT3 D	GCCCCATAGTATCTCAACATCA
oJH1327	RAD52 UP45 2	TTGCCAAGAACTGCTGAAGGTTCTGGTGGCTTTGGTGTGTTGTTGGAATTCG AGCTCGTTTAAAC
oJH1328	RAD52 DN45 2	TAAATAATGATGCAAATTTTTTATTTGTTTCGGCCAGGAAGCGTTCGGATCCC CGGGTTAATTAAG
oJH1239	RAD52 C2	TAGGCACACCGTTGATCAGA
oJH1240	RAD52 D2	CACATGGAGGAAAGAAAAACTAGA
oAW88	SAC3 UP45	TGTTGGTACTCATTTCAGGTAATACTCTTGGAAGGTATCCCTTAACGGATCCC CGGGTTAATTAAG
oAW89	SAC3 DN45	TATAGAAAAAATGCACATTTCTTTTGTTTATATATTACAAATGCTGAATTCGAG CTCGTTTAAAC
oAW90	SAC3 C	CCGTATTACCCGTTAGCACA
oAW91	SAC3 D	CGCCGACAGTAATAAGAAATG
oAZ110	TRP1 UP	CATGGAGGGCGTTATTACG
oAZ111	TRP1 DN	CCGCTAATAGGAAGTATGAATACC
oAZ112	TRP1 C	GAGACCGAGTTAGGGACAGTTAG
oAZ113	TRP1 D	AGCGAAAAGACGATAAATACAAG
oJH1520	TOM70 DN45 1	TAGTTTTTGTCTTCTCCTAAAAGTTTTTAAGTTTATGTTTACTGT GAATTCGAGCTCGTTTAAAC
oJH1521	TOM70 UP45 1	AAGATTCAAGAAACTTTAGCTAAATTACGCGAACAGGGTTTAATG CGG ATC CCC GGG TTA ATT AAC
oJH1522	TOM70 C	AAGTTGGATGGTATTTATGTTGGA
oJH1523	TOM70 D	GAACATGCATACGTGTATATTGAAAC
oDH11	RPL13A-mCherry UP45	AAGAGAGCTAGAGAAAAGGCTGAAGCTGAAGCTGAAAAGAAGAAATGCATGC TTATGGTGAGCAA
oDH12	RPL13A-mCherry DN45	ATACAAAAATTGTGGATGAAAAATTCTTTGATGAAGTTTTTAGATAAGTTATAC TAGTTCGTCGACTGGAT
oDH8	RPL13A C	CAGAACCTTGAGATTAGCCAGAT
oDH9	RPL13A D	ATCTTTCGCATCTCTTCTATGC
oJH1819	pFA6a I-SceI fix F	ATAGATCTGTTTAGCTTGCCTCG
oJH1820	pFA6a I-SceI fix R	GCGGATCTGCCGGTAGAG
oJH1808	ChrXII insert UP45 1	GTGTTTATCAGATCAGTGTGATGTGTTCAGCTAAATGGAAAGCTA CCGCGCGTTGGCCGATTCAT
oJH1809	ChrXII insert DN45 1	TACTGTGAGACCTTTTCTTGCAATATCTCGATCAGATAGCATCTG TTCGTACGCTGCAGGTCGAC
oJH1798	Chr V-XII inversion F1	GTCACATTGA GAGCTCCCGCTCTTTTTCAAAC
oJH1799	Chr V-XII inversion R1	GTCACATTGA GGATC CGATACAGTGTTCCAGAATTGTCA
oJH1800	Chr V-XII inversion F2	GTCACATTGA GGATCC TAGGGATAACAGGG TAATCCCAAATAATGTATGTAGAATAGA
oJH1801	Chr V-Xii inversion R2	GTCACATTGA CCGCGG AGGTATGTCATCGTAATCAAGT

Table S2: Oligonucleotides used in this work

pJH9	pFA6a TRP1	(Longtine et al., 1998)
pJH20	pFA6a GFP HIS3	(Longtine et al., 1998)
pJH369	pAW8-mCherry	(Watson et al., 2008)
pJH388	pFA6a-GFP-KanMX6 no I-SceI	I-SceI site removed by site directed mutagenesis
pJH381	pGSTU	delitto perfetto plasmid with Kan swapped out for TRP1
pJH387	pGST-V-U	For reciprocal translocations with Chr V sub-telomere. Has region of V:564025-566025 inserted between URA3 and TRP1 markers with SceI site in the middle. Note plasmid yield was weirdly low
pJH73	pFA6a URA3	(Houseley and Tollervey, 2011)

Table S3: Plasmids used in this work